HHS Public Access

Author manuscript

Nat Immunol. Author manuscript; available in PMC 2024 July 22.

Published in final edited form as:

Nat Immunol. 2023 August ; 24(8): 1358–1369. doi:10.1038/s41590-023-01540-y.

Distinct metabolic requirements regulate B cell activation and germinal center responses

Rahul Sharma[1], **Ryan M. Smolkin**[2,6], **Priyanka Chowdhury**[3,6], **Keith Conrad Fernandez**[3], **Youngjun Kim**[3], **Montserrat Cols**[1], **William Alread**[1], **Wei-Feng Yen**[1], **Wei Hu**[1], **Zhong-Min Wang**[2], **Sara Violante**[4], **Ronan Chaligné**[5], **Ming O. Li**[1,2,3], **Justin R. Cross**[4], **Jayanta Chaudhuri**[1,2,3]

[1]Immunology Program, Sloan Kettering Institute, Memorial Sloan Kettering Cancer Center, New York, NY, USA.

[2]Gerstner Sloan Kettering Graduate School of Biomedical Sciences, New York, NY, USA.

[3]Immunology and Microbial Pathogenesis Program, Weill Cornell Graduate School of Medical Sciences, New York, NY, USA.

[4]Donald B. and Catherine C. Marron Cancer Metabolism Center, Memorial Sloan Kettering Cancer Center, New York, NY, USA.

[5]Computational and Systems Biology Program, Sloan Kettering Institute, Memorial Sloan Kettering Cancer Center, New York, NY, USA.

[6]These authors contributed equally: Ryan M Smolkin, Priyanka Chowdhury.

Abstract

Following infection or vaccination, activated B cells at extrafollicular sites or within germinal centers (GCs) undergo vigorous clonal proliferation. Proliferating lymphocytes have been shown to undertake lactate dehydrogenase A (LDHA)-dependent aerobic glycolysis; however, the specific role of this metabolic pathway in a B cell transitioning from a naïve to a highly proliferative, activated state remains poorly defined. Here, we deleted LDHA in a stage-specific and cell-specific manner. We find that ablation of LDHA in a naïve B cell did not profoundly affect its ability to undergo a bacterial lipopolysaccharide-induced extrafollicular B cell response. On the other hand, LDHA-deleted naïve B cells had a severe defect in their capacities to

Correspondence and requests for materials should be addressed to Jayanta Chaudhuri. chaudhuj@mskcc.org.

Author contributions

R.S. and J.C. conceptualized the work, analyzed the data and wrote the manuscript; R.M.S., P.C., K.C.F., Y.K., M.C., W.-F.Y., W.H., Z.-M.W. and S.V. collected, analyzed and validated data; R.M.S. and R.C. analyzed and interpreted scRNA-seq data; R.M.S. and K.C.F. conceptualized and carried out sequencing for the SHM assay; W.A. genotyped mice and made general reagents for experiments; M.O.L. generated conditional *Ldha* mice; J.R.C. analyzed data on B cell metabolism.

Competing interests

The authors declare no competing interests.

Additional information

Extended data is available for this paper at https://doi.org/10.1038/s41590-023-01540-y.

Supplementary information The online version contains supplementary material available at https://doi.org/10.1038/s41590-023-01540-y.

form GCs and mount GC-dependent antibody responses. In addition, loss of LDHA in T cells severely compromised B cell-dependent immune responses. Strikingly, when LDHA was deleted in activated, as opposed to naïve, B cells, there were only minimal effects on the GC reaction and in the generation of high-affinity antibodies. These findings strongly suggest that naïve and activated B cells have distinct metabolic requirements that are further regulated by niche and cellular interactions.

To mount a robust and durable humoral response following infection or immunization, antigen-activated B cells participate in T cell-dependent GC and T cell-independent extrafollicular (EF) responses[1]. During the latter, activated B cells migrate to the EF regions of secondary lymphoid organs and rapidly divide and differentiate into mitotically cycling, low-affinity antibody-secreting plasmablasts[1]. Around the same time, a subset of the activated B cells migrates into B cell follicles where they interact with cognate $CD4^+$ follicular helper T (T_{FH}) cells, undergo activation-induced cytidine deaminase (AID)-driven class-switch recombination and subsequently differentiate into GC B cells[2,3]. Within the GCs, activated B cells undergo AID-dependent somatic hypermutation (SHM) and rapid clonal proliferation in the dark zone (DZ), with selection of high-affinity B cell clones occurring in the light zone (LZ)[2]. Since both the EF and the GC responses involve rapid B cell proliferation, they have exigent metabolic demands for energy and biomass generation.

In general, non-proliferating cells convert glucose into pyruvate that is shunted into the mitochondrial tricarboxylic acid cycle to generate reducing equivalents for fueling ATP production via oxidative phosphorylation (OxPhos)[4–6]. On the other hand, in a phenomenon first discovered in cancer cells and termed the Warburg effect[7], proliferating cells such as activated T cells undergo aerobic glycolysis wherein pyruvate is converted to lactate even in the presence of oxygen[4,8,9]. The conversion of pyruvate to lactate is catalyzed by the lactate dehydrogenase (LDH) enzymes, which are tetrameric complexes comprising LDHA and/or LDHB subunits forming one of five isozymes (A_4B_0, A_3B_1, A_2B_2, A_1B_3 and A_0B_4)[8]. Recent studies have shown that LDHA is the primary isoform that is induced in activated $CD4^+$T cells, and LDH activity is manifested via the A_4B_0 form[8]. LDHA-deficient $CD8^+$ T cells exhibited severe defects in activation and proliferation[10], while deletion of *Ldha* in $CD4^+$ T cells led to altered T_H17 differentiation[11,12]. In the context of GCs, T_{FH} cells play a major role in the selection of high-affinity B cells[13]; however, the metabolism-governed role of T cells on B cell responses remains unresolved. Overall, the roles of LDHA-mediated glycolysis during B cell activation, proliferation and differentiation remain poorly defined.

B cells have distinct metabolic requirements during development and activation[14]. Upon B cell receptor (BCR) cross-linking or T cell-mediated stimulation via CD40–CD40 ligand interactions, activated B cells upregulate the Glut family of glucose transporters to promote glucose uptake and glycolysis[15–17]. GC B cells also show increased glucose uptake and high mitochondrial content, suggesting intense metabolic activity[18]. Additionally, the LZs of GCs were found to be hypoxic, an environment that would theoretically facilitate glycolysis and influence GC-based antibody responses[19]. Despite these observations and the widely accepted notion that proliferating lymphocytes upregulate glycolysis, GC B cells were shown to carry out minimal glycolysis and instead to rely on fatty acid oxidation[20].

Additionally, OxPhos was shown to fuel the metabolic demands of high-affinity GC B cell clones[21,22]. Thus, despite increased glucose uptake, the role of aerobic glycolysis during a GC response remains poorly defined. Likewise, a B cell activated ex vivo under conditions that simulate an EF response increases glucose uptake and upregulates both aerobic glycolysis and OxPhos[15,23,24]. However, the requirement for aerobic glycolysis during a T cell-independent response in vivo remains elusive. Thus, the metabolic reprogramming that B cells experience as they transition from a naïve to an activated state, undergoing a GC response or an EF response, is yet to be elucidated.

Here, we have deleted LDHA in a cell-specific and stage-specific manner and find that its ablation in naive B cells, before their activation, leads to a profound defect in the proliferation of pre-GC B cells, formation of mature GCs, and generation of GC-dependent antibody responses. Likewise, loss of LDHA in T cells severely compromises the ability of B cells to mount a GC response. Surprisingly, when LDHA was deleted in activated, as opposed to naïve, B cells, there was only a minimal effect on the GC response and on the generation of high-affinity antibodies. Additionally, LDHA and, by extension, aerobic glycolysis, appear to play a minimal role in B cells undergoing a T cell-independent EF response. These results support the notion that a robust humoral response relies on distinct metabolic programs that are influenced by the fates B cells have adopted following activation. Metabolism-governed cell-fate choices further modulated by cellular niche and heterocellular interactions reveal differential metabolic requirements of B cells during their transitions from naïve to activated states.

Results

LDHA influences aerobic glycolysis in B cells

By catalyzing the conversion of pyruvate to lactate while regenerating NAD^+ from NADH, LDHA participates in a key step of aerobic glycolysis[25]. To determine the requirement for LDHA in B cell function, we generated $Ldha^{fl/fl}Cd23^{Cre}$ mice wherein the $Cd23^{Cre}$ transgene drives expression of the Cre recombinase in some transitional B cells, as well as in marginal zone (MZ) and follicular (FO) B cells[26]. Analysis of naïve and activated splenic B cells from $Ldha^{fl/fl}Cd23^{Cre}$ mice showed efficient deletion of the floxed exon (exon 3)[8], loss of the *Ldha* transcript and absence of the LDHA protein (Extended Data Fig. 1a–c).

To examine how loss of LDHA affects glycolytic flux, we activated splenic B cells with cocktails of cytokines and activators that simulate B cell activation in vivo[27] and determined the extracellular acidification rate (ECAR), an indicator of glycolysis[4], with a Seahorse analyzer (Fig. 1a). Control ($Ldha^{+/+}Cd23^{Cre}$) B cells cultured in glucose-deprived media increased ECAR after addition of glucose (Fig. 1b–e), indicating that the cells can undergo aerobic glycolysis. On the other hand, $Ldha^{fl/fl}$ $Cd23^{Cre}$ B cells cultured in glucose-deprived media did not increase ECAR to the same level as that of control cells after addition of glucose (Fig. 1b–e), suggesting that loss of LDHA impaired the ability of B cells to induce glycolysis. As expected, LDHA-deficient B cells activated ex vivo showed a marked reduction in lactate production (Fig. 1f). However, both the residual ECAR and lactate production observed in LDHA-deficient B cells suggest that glycolysis is not completely abolished. To examine if LDHB could account for this residual glycolytic activity that can

compensate for the lost glycolytic potential in B cells as in cancer cells[28], we carried out quantitative PCR analysis but failed to detect expression of *Ldhb* either in naïve or in activated B cells (Extended Data Fig. 1d). It is possible that the lingering LDHA protein in *Ldha*$^{fl/fl}$*Cd23*^{Cre} B cells could allow facilitate a low level of glycolysis, or that there exists an unidentified LDHA-independent backup pathway used by B cells to engage in low levels of glycolysis.

Unlike the marked effect on aerobic glycolysis, loss of LDHA in B cells did not lead to statistically significant changes to their oxygen consumption rate and spare respiratory capacity, two indicators of mitochondrial OxPhos (Extended Data Fig. 2a–e). Uptake of the fluorescent glucose analog 2-NBDG was similar between *Ldha*$^{fl/fl}$*Cd23*^{Cre} and control B cells (Extended Data Fig. 3a) and the observed differences in intracellular ATP levels were not statistically significant (Extended Data Fig. 3b), suggesting that the majority of cellular ATP in B cells is generated in an LDHA-independent manner. Despite these similarities, activated *Ldha*$^{fl/fl}$*Cd23*^{Cre} B cells failed to proliferate ex vivo when cultured with lipopolysaccharide (LPS) + interleukin-4 (IL-4; Extended Data Fig. 3c,d) or with LPS + transforming growth factor-β + anti-IgD (Extended Data Fig. 3e), likely due to their impaired ability to engage in aerobic glycolysis.

In the spleen, LDHA deficiency did not grossly affect the frequencies of immature transitional T1, T2 and T3 B cells[29], in which small but statistically insignificant differences were evident (Extended Data Fig. 4a,b). The frequency of B1a B cells in the peritoneum of *Ldha*$^{fl/fl}$ *Cd23*^{Cre} mice was moderately increased relative to control mice (Extended Data Fig. 4c,d). It is, however, unclear if the *Cd23*^{cre} transgene efficiently deleted *Ldha* in all transitional or B1a B cells. The frequency of FO B cells in the spleen did not differ between the *Ldha*$^{fl/fl}$*Cd23*^{Cre} mice and control group, despite modest differences in their absolute numbers (Extended Data Fig. 4e–g). The frequency of splenic MZ B cells was similar in all the mice examined (Extended Data Fig. 4e,h). However, there was a modest but statistically significant increase in the absolute numbers of MZ B cells in *Ldha*$^{fl/fl}$*Cd23*^{Cre} mice (Extended Data Fig. 4e,i). The reason for this difference is currently unclear. Finally, the frequencies of CD4^{+} and CD8^{+} T cells in the blood and spleen were similar in the *Ldha*$^{fl/fl}$*Cd23*^{Cre} mice and control animals (Extended Data Fig. 4j,k). Thus, the loss of LDHA in naïve B cells did not have an effect on the number and on the frequency of mature B cells at homeostasis, allowing us to use *Ldha*$^{fl/fl}$*Cd23*^{Cre} mice as a tool to explore the role of LDHA, and consequently, aerobic glycolysis, in B cell activation.

LDHA is largely dispensable for an extrafollicular response

To examine if LDHA deficiency impacts the EF arm of the humoral immune response, we used an in vivo model wherein B cell activation occurs through a Toll-like receptor (TLR) 4-dependent, BCR-independent pathway[30] (Fig. 2a). In this model, mice challenged intravenously with LPS exhibit a rapid expansion of activated GL7^{+} B cells in the spleen, along with an increase in the frequencies of IgG3^{+} class-switched B cells and of CD138^{+} plasmablasts[31]. We observed that at day (d) 5 after administration of LPS, the frequency of IgG3^{+} class-switched B cells in the spleen was similar between *Ldha*$^{fl/fl}$*Cd23*^{Cre} mice and control mice (Fig. 2b,c and Extended Data Fig. 5a). We also observed that CD138^{+}

plasmablasts were induced in the spleens of LPS-challenged *Ldha*$^{fl/fl}$*Cd23*^{Cre} mice to nearly the same frequency as that in *Cd23*^{Cre} control mice; the trend toward reduced plasmablast frequency in *Ldha*$^{fl/fl}$*Cd23*^{Cre} mice did not reach statistical significance (Fig. 2d,e). Unperturbed IgG3 switching in the spleens of LPS-challenged *Ldha*$^{fl/fl}$*Cd23*^{Cre} mice suggests that B cell activation and proliferation were generally not affected by LDHA deficiency. Indeed, Ki67 staining showed that the loss of LDHA did not have a statistically significant effect on the frequency of either GL7^{+} (activated) or GL7^{-} (unactivated) B cells undergoing proliferation in LPS-challenged mice (Fig. 2f). A critical metabolic parameter, mTORC1 activity, serves as an indicator of B cell activation[19]. The frequency of phosphorylated S6^{+} cells, a surrogate for mTORC1 activity, among GL7^{+} or GL7^{-} B cells was similar between LDHA-sufficient and LDHA-deficient mice (Fig. 2g).

Finally, we analyzed serum antibodies following LPS injection. While we did not observe an appreciable boost in serum IgG3 levels, there was an approximately tenfold induction of serum IgM in *Ldha*$^{+/+}$*Cd23*^{Cre} control mice upon LPS administration, with a smaller increase in *Ldha*$^{fl/fl}$*Cd23*^{Cre} mice (Fig. 2h). Genomic PCR analysis of CD138^{+} B cells sorted from *Ldha*$^{fl/fl}$*Cd23*^{Cre} mice following LPS challenge confirmed the deletion of the *Ldha*$^{fl/fl}$ allele (Extended Data Fig. 5b). Additionally, when FO and MZ B cells were sorted and activated ex vivo, the IgM titers in the culture supernatants were similar between *Ldha*$^{fl/fl}$*Cd23*^{Cre} and controls; the trend toward higher IgM titers in the supernatants of *Ldha*$^{fl/fl}$*Cd23*^{Cre} MZ B cells was not statistically significant (Extended Data Fig. 5c). Genomic PCR analysis of these MZ B cells confirmed the deletion of the *Ldha*$^{fl/fl}$ allele (Extended Data Fig. 5d). *Ldha*-deleted B cells in vivo responded differently from those in ex vivo experiments wherein LDHA-deficient B cells stimulated with LPS + IL-4 or with anti-IgD-mediated BCR cross-linking did not proliferate (Extended Data Fig. 3c–e). This difference is likely due to the presence of factors such as BAFF and APRIL in the B cell milieu in vivo that promote B cell survival[32]. Overall, these results suggest that LDHA is largely dispensable for the rapid B cell activation in an LPS-challenge model that likely represents a T cell-independent EF B cell response.

LDHA is essential for germinal center-mediated responses

The lack of an overt LDHA dependency in a T cell-independent EF B cell response prompted us to examine the requirement for LDHA in a T cell-dependent GC humoral response. A GC-dependent B cell response requires antigen recognition, cellular activation, class switching, interactions with FO dendritic cells and T_{FH} cells, SHM and affinity maturation[2], with each of these steps potentially having specific metabolic requirements. Thus, the metabolic fitness of a B cell may determine its ability to engage in a GC reaction[33].

We first examined GC B cells in the Peyer's patches (PPs) of *Ldha*$^{fl/fl}$*Cd23*^{Cre} mice. Within the gut, B cells in the PPs are continuously engaged both by the intestinal microbiota and by food antigens. This makes the PPs ideal sites to examine the state of activated B cells at homeostasis[34]. We observed that the frequency of GC B cells (B220^{+}GL7^{+}Fas^{+}; gating strategy shown in Extended Data Fig. 6a) in the PPs of *Ldha*$^{fl/fl}$*Cd23*^{Cre} mice was markedly reduced compared to *Ldha*$^{+/fl}$ *Cd23*^{Cre} mice and *Cd23*^{Cre} control animals (Fig. 3a,b). In

keeping with the impaired GC response, the serum of *Ldha*$^{fl/fl}$*Cd23*^{Cre} mice had greatly reduced levels of IgG1 and IgA isotypes relative to control mice; the IgM concentration in the serum, however, was unaffected (Fig. 3c). These findings suggest that LDHA deficiency affects the ability of B cells to mount a robust homeostatic immune response.

To determine if LDHA plays a role in GC responses following immunization, we immunized mice with NP-CGG, wherein the hapten NP (4-hydroxy-3-nitrophenylacetyl) conjugated to chicken γ-globulin induces a robust T-dependent humoral response[35] (Fig. 3d). We observed that at d14 after immunization, both the frequency and the absolute number of GC B cells in *Ldha*$^{fl/fl}$*Cd23*^{Cre} mice were severely reduced compared to control mice (Fig. 3e). Immunofluorescence microscopy revealed that immunized *Ldha*$^{fl/fl}$*Cd23*^{Cre} mice had smaller and fewer GCs within the follicles relative to controls (Fig. 3f and Extended Data Fig. 6b). The sera of *Ldha*$^{fl/fl}$*Cd23*^{Cre} mice had negligible titers of high-affinity (NP_8) and all-affinity (NP_{30}) anti-NP IgM and IgG1 antibodies, suggesting a severe defect in affinity maturation or antigen-specific antibody production (Fig. 3g,h). Finally, we carried out mixed bone marrow chimera experiments and observed that *Ldha*$^{fl/fl}$*Cd23*^{Cre} B cells failed to compete successfully with control B cells in contributing to the GC pool in the spleens of NP-CGG-immunized mice (Fig. 3i). Thus, in stark contrast to the general dispensability of LDHA for mounting a T cell-independent EF response, loss of LDHA in mature B cells impairs their ability to mount a T cell-dependent GC response.

LDHA is required for pre-germinal center B cell proliferation

The severe abrogation of a T cell-dependent GC response in *Ldha*$^{fl/fl}$ *Cd23*^{Cre} B cells led us to examine the effects of LDHA deletion during the early phase of the humoral response. To this end, we immunized *Ldha*$^{fl/fl}$*Cd23*^{Cre} and control mice with a single dose of NP-CGG (without boost) and measured the relative titers of all-affinity and high-affinity IgM and IgG1 antibodies at days 0 (pre-immunization), 4, 7 and 10. Paralleling the defect of the mature GC response, the antibody titers of *Ldha*$^{fl/fl}$*Cd23*^{Cre} mice were severely diminished for both all-affinity and high-affinity antibody isotypes (Fig. 4a–d). These results indicate that loss of LDHA in B cells leads to a defect in the early GC response following immunization.

To decipher the nature of this defect in greater detail, we analyzed pre-GC B cells, which we defined as GL7$^+$ B cells at d4 following immunization. The frequency of pre-GC B cells in immunized mice, while low, was higher than that observed in PBS controls (Extended Data Fig. 6c). We enriched for GL7$^+$ (activated) and GL7$^-$ (naive) B cells from *Ldha*$^{fl/fl}$*Cd23*^{Cre} and from *Cd23*^{Cre} control mice at d4 after NP-CGG immunization (Extended Data Fig. 6d). Post-sort analysis showed that while the naïve B cells formed a tight GL7$^-$ population, a large fraction of the sorted GL7$^+$ population fell into the GL7$^-$ gate. This is likely due to the less stringent gating strategy that was used to recover the relatively sparse activated B cells at this early time point following immunization, or that a fraction of the activated B cells lost GL7 positivity following sorting. The sorted GL7$^+$ and GL7$^-$cells were mixed at a 3:1 ratio and processed for 5′-end single-cell RNA sequencing (scRNA-seq). Dimensionality reduction and principal component analysis identified four major cell clusters (Fig. 4e):clusters 1 and 2 were similar to one another, yet both clusters

are distinct from the ribosomal protein cluster. While the majority of the sequenced GL7^{-} cells probably lie within these three clusters, the cells did not segregate based on their *Ldha* genotype. Of the four clusters, only the proliferating cluster, defined by the expression of *Mki67* and *Top2a*, was markedly reduced in *Ldha*$^{fl/fl}$*Cd23*^{Cre} mice.

To determine if cell activation was impaired in the *Ldha*$^{fl/fl}$*Cd23*^{Cre} mice, we compared *Bcl6* expression and observed that it was equivalent between the non-proliferating *Ldha*$^{fl/fl}$*Cd23*^{Cre} and control B cells. *Bcl6* expression was elevated in the proliferating cluster, although the cells with the highest expression were absent from the *Ldha*$^{fl/fl}$*Cd23*^{Cre} mice (Fig. 4f,g). CCR6 is a chemokine receptor that regulates the kinetics and the efficiency of the initiation of the GC reaction, with cells expressing it potentially representing a transitional stage between naïve and GC B cell phenotypes[36,37]. We observed that Ccr6 expression was similar between *Ldha*$^{fl/fl}$*Cd23*^{Cre} and control B cells in both the proliferating and non-proliferating subsets (Fig. 4h,i). Additionally, we observed BCR mutations primarily in the proliferating pre-GC population of control B cells (Fig. 4j), implying that while the loss of LDHA in naive B cells may not prevent their activation, it does abrogate GC dynamics. While we could not entirely rule out an epigenetic defect, our results suggest that deletion of *Ldha* leads to a proliferative defect in early GC precursors that underlies the perturbed antibody responses in *Ldha*$^{fl/fl}$*Cd23*^{Cre} mice.

LDHA in T cells is essential for B cell germinal center responses

A robust GC reaction requires cognate interactions between antigen-specific B cells and T_{FH} cells[2]. Because LDHA in B cells appears to play a major role in T cell-dependent immune responses and both the cell types reside in similar cellular niches, we examined the potential T cell-specific role of LDHA in influencing the GC reaction. We therefore generated *Ldha*$^{fl/fl}$*Cd4*^{Cre} mice and observed that deletion of *Ldha* in T cells affected neither the frequency ($P = 0.3921$; Fig. 5a) nor the number ($P = 0.2736$; Fig. 5b) of T_{FH} cells in the spleens of NP-CGG-immunized mice. However, the frequency of GC B cells (Fig. 5c), the absolute number of GC B cells (Fig. 5d) and the frequency of NP-specific GC B cells were greatly reduced (Fig. 5e). Consistent with the broad defect in the GC response, we observed that the titers of low-affinity (Fig. 5f) and affinity-matured (Fig. 5g) IgM and IgG1 antibodies were markedly reduced in the sera of *Ldha*$^{fl/fl}$*Cd4*^{Cre} mice relative to controls. Immunofluorescence studies revealed an abrogated GC formation in *Ldha*$^{fl/fl}$ *Cd4*^{Cre} mice following immunization (Extended Data Fig. 7a).

To examine if T_{FH} cells lacking LDHA were intrinsically compromised in providing help to B cells, we co-cultured sorted T_{FH} cells from immunized *Ldha*$^{fl/fl}$*Cd4*^{Cre} and control mice with antigen-primed B cells[38]. Even though there were fewer *Ldha*-deleted T_{FH} cells at d6 of co-culture relative to control T_{FH} cells, the absolute numbers of B cells were similar in both co-cultures (Extended Data Fig. 7b,c). However, the titers of IgM and IgG1 antibodies in the co-culture supernatant of *Ldha*-deleted T_{FH} cells were reduced relative to those detected in the co-culture supernatant of control T_{FH} cells (Extended Data Fig. 7d,e). These results show that *Ldha*-deleted T_{FH} cells are defective in providing optimum help to B cells and could explain the severe deficiency in the GC responses of *Ldha*$^{fl/fl}$*Cd4*^{Cre} mice.

In contrast to the effect on GC-dependent humoral response, loss of LDHA in T cells did not alter the ability of B cells to mount an EF response. The frequencies of IgG3-switched B cells and of $CD138^+$ plasmablasts in the spleen were similar between $Ldha^{fl/fl}Cd4^{Cre}$ mice and controls (Fig. 5h,i). We also observed that the serum concentrations of IgM and IgG3 antibodies following LPS injection were largely comparable across all the mice studied (Fig. 5j). Moreover, loss of LDHA in T cells did not affect B cell proliferation and mTORC1 activity upon LPS challenge (Extended Data Fig. 8a,b) and the frequencies and the proliferative capacities of $CD4^+$ and $CD8^+$ T cells (Extended Data Fig. 8c,d). Additionally, there was no change in the frequencies of naïve ($CD62L^{hi}$ $CD44^{lo}$), central memory ($CD62L^{hi}CD44^{hi}$) or effector ($CD62L^{lo}CD44^{hi}$) populations of either $CD4^+$ or $CD8^+$ T cells in the LPS-challenged $Ldha^{fl/fl}Cd4^{Cre}$ mice (Extended Data Fig. 8e). Taken together, deletion of LDHA in T cells had a dramatic but context-dependent effect on B cells, wherein the GC B cell response was severely impaired, but the EF response was unaffected.

Requirement of LDHA in germinal center B cells

Because one of the hallmarks of lymphocyte activation is activation-induced metabolic reprogramming[39], we wanted to examine the role of LDHA-dependent glycolysis after a B cell has been activated. To this end, we conditionally deleted LDHA in activated B cells by breeding $Ldha^{fl/fl}$ mice to $Aicda^{Cre}$ mice[40]. Unlike the $Cd23^{Cre}$ transgene that is expressed in naïve B cells[26], $Aicda^{Cre}$ is expressed in activated B cells at the boundary between T zones and B cell follicles (T–B border) before their eventual migration into the GCs[3]. We reasoned that comparing the humoral responses of $Ldha^{fl/fl}Aicda^{Cre/+}$ mice to those observed in $Ldha^{fl/fl}Cd23^{Cre}$ animals would enable us to distinguish between the potentially dissimilar consequences arising from the loss of LDHA in naïve B cells before their activation versus its deletion following activation. We observed that PPs of $Ldha^{fl/fl}Aicda^{Cre/+}$ mice had a 25% decrease in the frequency of GC B cells, relative to $Ldha^{+/+}Aicda^{Cre/+}$ control animals (Fig. 6a,b), in contrast to the 80% reduction in the frequency of GC B cells in the PPs of $Ldha^{fl/fl}Cd23^{Cre}$ mice (Fig. 3a,b). Additionally, the frequency of IgA^+ GC B cells in the PPs (Fig. 6b) and the titers of IgM, IgG1 and IgA antibodies in the sera of $Ldha^{fl/fl}Aicda^{Cre/+}$ mice were largely similar to those of control animals at homeostasis (Fig. 6c).

To examine the NP-specific humoral response, we immunized $Ldha^{fl/fl}Aicda^{Cre/+}$ mice and control mice with NP-CGG. We observed that the frequency of GC B cells in $Ldha^{fl/fl}Aicda^{Cre/+}$ mice was slightly lower than in control animals; however, the difference was not statistically significant ($P = 0.4576$; Fig. 6d). On the other hand, the absolute number of GC B cells (Fig. 6e), the frequency of NP-specific B cells (Fig. 6f), the frequencies of DZ and LZ B cells (Fig. 6g) and the frequency of $IgG1^+$ class-switched GC B cells (Fig. 6h) were all largely similar between $Ldha^{fl/fl}$ $Aicda^{Cre/+}$ and control mice. In addition, GC cell viability (Extended Data Fig. 9a), cell size (Extended Data Fig. 9b), mitochondrial content and function (Extended Data Fig. 9c,d) and cell-cycle progression as assessed by incorporation of the nucleoside analog BrdU (Fig. 7a,b) were similar in mice of both genotypes. Furthermore, serum antibody analysis over a time course of 28 d revealed no differences in the relative titers of all-affinity or of high-affinity IgM antibodies (Fig. 7c,d).

While NP-specific IgG1 levels were lower in *Ldha*$^{fl/fl}$*Aicda*$^{Cre/+}$ mice relative to controls at earlier time points, the levels were similar from d14 onwards (Fig. 7e,f), suggesting that LDHA is dispensable for affinity maturation of antibodies.

PCR analysis of the genomic DNA and immunoblot assay showed efficient deletion of *Ldha* in *Ldha*$^{fl/fl}$*Aicda*$^{Cre/+}$ GC B cells, suggesting that the GCs were not largely populated by LDHA-sufficient B cells that have escaped genetic deletion (Extended Data Fig. 9e,f). Furthermore, RNA-seq data showed that *Ldhb* was not expressed in either wild-type or *Ldha*$^{fl/fl}$*Aicda*$^{Cre/+}$ GC B cells (Extended Data Fig. 9g), suggesting that LDHB does not compensate for the absence of LDHA in these GC B cells. Finally, we sequenced the *IgH* J_H4 intron from GC B cells of immunized mice. A mutation in the J_H4 intron is commonly used as a surrogate for variable region SHM[41], independent of affinity-based selection. We observed that the frequency of J_H4 mutations was similar between *Ldha*$^{fl/fl}$*Aicda*$^{Cre/+}$ mice and control mice (Fig. 7g). As SHM proceeds through proliferation in the DZ and LZ/DZ cycling of GC B cells, the generally unperturbed frequency of J_H4 mutations strongly suggests that loss of LDHA in B cells post-activation does not impact GC dynamics. Taken together, these results strongly support the notion that LDHA is dispensable in B cells after activation for a T cell-dependent immune response, in stark contrast to its essential role in the activation of a naïve B cell poised to undergo a GC reaction (Extended Data Fig. 10).

Discussion

In this work, we have deleted *Ldha* either in naïve or in activated B cells to determine its requirement at different stages of the humoral immune response. Our results show that naïve B cells activated ex vivo engage in LDHA-dependent aerobic glycolysis and that loss of LDHA markedly reduces ECAR and lactate production. Thus, despite the low level of aerobic glycolysis observed in LDHA-deficient B cells, in all likelihood, the requirement for LDHA at different stages of B cell activation reflects the necessity for aerobic glycolysis as opposed to a novel role of this protein. However, this latter possibility, although remote, cannot be ruled out and we have therefore exercised some degree of caution when suggesting that the loss of LDHA is a bona fide surrogate for loss of aerobic glycolysis.

While it is now established that activated lymphocytes such as T cells and NK cells undergo aerobic glycolysis[8,10–12,42], the role of this metabolic pathway at the distinct stages of B cell activation and differentiation during a humoral immune response has remained elusive. Here, we demonstrate that the requirement for LDHA in vivo is depends on the course that an antigen-stimulated B cell has undertaken following its initial activation. We find that B cells poised to undergo a GC response require LDHA. On the other hand, once activated, a ‘metabolic switch’ allows the activation-dependent transition of B cells from LDHA-dependent glycolysis to other metabolic pathways depending on the cell-fate choice a B cell has undertaken.

Our scRNA-seq data show that inactivation of LDHA in naïve B cells markedly impairs their proliferation at a very early stage of the GC response. Why is LDHA needed for B cells to initiate the GC response? Resting B cells have been shown to exist in partially

activated states[43], and once activated, build up their intracellular levels of precursors, such as nucleotides, before undergoing proliferation[44,45]. By regenerating NAD^+ that serves as an essential cofactor for the glycolytic enzyme glyceraldehyde-3-phosphate dehydrogenase, and by rapidly metabolizing the cytoplasmic buildup of pyruvate that can otherwise inhibit pyruvate dehydrogenase, aerobic glycolysis maintains the glycolytic flux required for both macromolecular biosynthesis as well as for energy production[9]. Additionally, by generating a positive glycolytic flux, aerobic glycolysis could potentially provide a rapid source of cytoplasmic ATP that can serve as a phosphate donor for phosphatidylinositol triphosphate generation[10,12]. This, in turn, would activate the signaling cascades that accompany B cell stimulation[46]. Overall, a B cell likely balances the competing needs of generating macromolecular intermediates, maintaining signaling activities and meeting cellular energetic demands by skewing the metabolic flux toward aerobic glycolysis at the expense of other metabolic pathways to effectively optimize the humoral response. Finally, recent studies have shown that lactate-derived histone lactylation could serve as an epigenetic modification to regulate gene expression in immune cells[47]. Overall, an antigen-activated B cell poised to undergo a T cell-dependent GC reaction could rely on LDHA for energy, macromolecular biosynthesis, signal transduction and epigenetic regulation, whereas the loss of LDHA could potentially affect one or more of these processes leading to a drastic defect in a GC response.

Why do activated B cells bypass the need for LDHA when they undergo an LPS-induced EF response? The proliferation and differentiation of B cells into antibody-secreting plasmablasts is accompanied by substantial increases in the number of layers and size of the endoplasmic reticulum and the Golgi network[48–51]. LPS-stimulated B lymphocytes have been demonstrated to undergo de novo lipogenesis[52], probably to synthesize the lipids and cholesterols necessary for the expansion of the antibody-secretory network. Thus, B cells differentiating into plasmablasts may downregulate aerobic glycolysis and instead metabolize glucose primarily through the Krebs cycle. Indeed, B cells upregulate oxidative metabolism prior to differentiation into plasmablasts[24] and as they mature into plasma cells, they import pyruvate into the mitochondria for long-term survival[53].

Our results demonstrate that B cells that have already initiated a GC response are less reliant on LDHA-dependent aerobic glycolysis as they have switched to utilizing other metabolic pathways, consistent with recent work showing that GC B cells selectively oxidize fatty acids for energy[20]. This shift may allow GC B cells to scavenge and utilize fatty acids from the abundant dying cells in their surroundings[20], allowing these B cells to switch from an energy-exclusive to an energy-inclusive state to meet the intense metabolic demands of rapid proliferation. Whether this metabolic reprogramming is initiated via LPS-mediated stimulation of TLR4 in conjunction with BCR cross-linking during an EF response or via the nature and the intensity of T_{FH} interactions during a GC response remains to be deciphered. Nevertheless, we cannot exclude the possibility that some GC B cells do engage in aerobic glycolysis under normal circumstances but are more metabolically flexible than non-GC B cells, permitting them to cope with the loss of *Ldha* by employing other metabolic pathways.

The loss of LDHA in T cells impairs their ability to sustain a GC response, suggesting that aerobic glycolysis is critical for T_{FH} cells to provide help to B cells. Co-culture experiments suggest that though LDHA-deficient T_{FH} cells can facilitate the proliferation of B cells, they cannot provide the stimulation required to convert the B cells into antibody-secreting plasmablasts. However, the mechanism by which LDHA influences the ability of T_{FH} cells to sustain a GC response needs further investigation.

The precise reason why B cells rely more on LDHA in one stage versus others is unclear at present. Naïve B cells could be metabolically heterogeneous, and their differential reliance on LDHA could in turn determine whether a B cell commits to an EF-dependent or GC-dependent pathway during the immune response. Such heterogeneity could ensure that at least one arm of the humoral immune response remains active during an infection in case there is a failure in mounting a GC-based response. Our scRNA-seq analysis of early GC B cells suggests that there might exist an evolutionary fail-safe mechanism to ensure that only B cells that are sufficiently metabolically flexible can undergo proliferative bursts to form a GC. The rapid switch from a glycolysis-dependent to a glycolysis-independent state may also act as a metabolic checkpoint to gauge the fitness of a B cell before it undergoes further iterative rounds of selection and proliferation in the GCs. Finally, the metabolic shift to a glycolysis-independent pathway could ensure that GC B cells undergoing affinity maturation and rapid proliferation do not metabolize high levels of glucose that, at least in early developing B cells, could promote their malignant transformation[54].

The temporal specificity of the cells in which this metabolic switch occurs is vital to understanding B lymphocyte fate choices and their regulation of immunity. By comparing, to matched wild-type cells, antigen-specific CRISPR-labeled cells wherein LDHA or another metabolic enzyme is deleted in a temporal- and stage-specific manner, we can ascertain whether the role of these metabolic enzymes is influenced by the cells' affinity for their cognate antigen or their maturation/activation state. We can further dissect the involvement of antigen receptor affinity in shaping the metabolic landscape of B cells by evaluating the humoral immune response in B-cell-specific metabolic gene-knockout mice expressing BCR of various specificities for NP. Similar experiments using T cells expressing a knocked-in TCR would clarify the manner by which metabolic processes influence the functional properties and impacts of T_{FH} cells on the quality of the B cell response.

Overall, our studies reveal a niche-dependent and activation-dependent metabolic reprogramming, which in turn leads to distinct immunological outcomes that might influence the formation of a robust and durable humoral response. The notion that metabolic checkpoints regulate the quality of a GC response reveals new paradigms in GC biology and further investigation is required to unravel the specific metabolic programs that are undertaken by high-affinity B cell clones synthesizing high-quality neutralizing antibodies. Such information may help us exploit B cell metabolic reprogramming to engineer and optimize B cell-based immune responses during tumor immunity and vaccine development.

Online content

Any methods, additional references, Nature Portfolio reporting summaries, source data, extended data, supplementary information, acknowledgements, peer review information;

details of author contributions and competing interests; and statements of data and code availability are available at https://doi.org/10.1038/s41590-023-01540-y.

Methods

Mice, immunization and in vivo treatment

Mice were maintained in a specific pathogen-free facility. Experiments were performed in accordance with Memorial Sloan Kettering Cancer Center (MSKCC) and Institutional Animal Care and Use Committee (IACUC) guidelines. Mice and procedures used in the study were ethically approved by MSKCC IACUC. Mice were housed with food and water and 12-h dark–light cycles. Male and female mice aged 8–12 weeks old were analyzed. The following mouse strains on a C57BL/6 background were used: *Ldha*$^{fl/fl}$ (ref. 8), *Aicda*^{Cre} (ref. 40), *Cd23*^{Cre} (ref. 26), B6.SJL (CD45.1, 002014, The Jackson Laboratory), RAG2$^{-/-}$ (008449, The Jackson Laboratory) and *Cd4*^{Cre} (ref. 55). For T cell-dependent responses, mice were immunized intraperitoneally with 50 μg of NP-CGG (N-5055-E (conjugation ratio>40), Biosearch Technologies) precipitated with Imject alum adjuvant (77161, Thermo Scientific), and boosted with 100 μg at d10 for analysis at d14. For T cell-independent responses, mice were injected intravenously with 50 μg LPS from *Salmonella minnesota* R595 TLRgrade (ALX-581–008-L001, Enzo Lifesciences) and analyzed at d5. All blood collection was performed by submandibular bleeding, and BD microtainer SST blood tubes (365967, BD Biosciences) were used for serum collection.

Antigens, antibodies, chemicals and detection reagents

Antibodies used in this study are described in Supplementary Table 1. For glucose-uptake studies, 2-NBDG was purchased from Thermo Fisher Scientific (N13195). For intracellular staining, cells were processed with the True-Nuclear Transcription Factor Buffer Set (424401, BioLegend) according to the manufacturer's instructions. For mitochondrial stains, MitoTracker Green FM (M7514, Thermo Fisher) and MitoSOX (M36008, Thermo Fisher) were used. Cells were resuspended in PBS, counterstained with indicated antibodies and incubated at 37 °C for 20 min. Following staining, the cells were immediately fixed with BD Cytofix/Cytoperm buffer (554722, BD Biosciences) for 20 min in FACS buffer at 4 °C.

Bone marrow chimeras

To generate mixed bone marrow chimeras, *Rag2*$^{-/-}$ mice aged 6–8 weeks (stock no. 008449, The Jackson Laboratory) were irradiated with two doses of 6.5 Gy γ-irradiation. About 2 × 10^6 bone marrow cells were mixed at a ratio of 1:1 and injected intravenously into *Rag2*$^{-/-}$ recipient mice. The mice were analyzed 8 weeks later after transplantation.

B cell purification and ex vivo activation

Spleens were mashed and passed through 70-μm cell strainers (352350, Falcon) to dissociate cells into single-cell suspensions. Red blood cells (RBCs) were lysed by resuspending in 2 ml lysis buffer (150 mM NH_4Cl, 10 mM $KHCO_3$, 0.1 mM EDTA, pH 7.5) for 5 min at 25 °C. The lysis reaction was quenched by adding five volumes of B cell media (RPMI 1640 + L-glutamine (11875, GIBCO) + 15% FBS (35–010-CV, Corning) + 1% penicillin–streptomycin (400–109, Gemini)). Following RBC lysis, B cells were isolated from total

splenocytes by incubating with CD43 (Ly-48) MicroBeads (130–049-801, Miltenyi Biotec) in MACS buffer (500 ml PBS, 0.5% BSA, 0.5 M EDTA) followed by negative selection using LS Columns (130–042-401, Miltenyi Biotec). Naïve B cells were seeded at 1×10^6 per ml of B cell media and cultured ex vivo with combinations of LPS (30 μg ml^{-1}; L4130, Sigma), IL-4 (25 ng ml^{-1}, 404-ML-010, R&D systems), anti-CD40 (50 ng ml^{-1}; 12–0401-82, eBioscience) and $F(ab')_2$ anti-IgM (2 μg ml^{-1}; 115–006-020, Jackson ImmunoResearch). Cells were analyzed at 24 or 48 h as indicated.

Flow cytometry and cell sorting

Total splenocytes or peripheral blood cells were resuspended in FACS buffer (PBS + 2.5% FBS) after dissociation into single-cell suspension (splenic samples) and RBC lysis (both sample types). For PPs, tissues were mashed and passed through 70-μm cell strainer (352350, Falcon) without RBC lysis. Total splenocytes were resuspended in 5 ml FACS buffer for downstream analysis. Around 150 μl of the splenocyte suspension was pipetted in each well of the 96-well round-bottom plate (08–772-17, Fisher). Cells were spun at 2,000*g* for 1 min at 4 °C and then resuspended in FACS buffer containing CD16/CD32 F_C blocking antibody (553142, BD) and Zombie Red viability dye (423109, BioLegend) for live/dead staining at 25 °C for 10 min. After F_C blocking, cells were washed twice in cold FACS buffer at 4 °C and stained with antibodies targeting surface proteins. For intracellular staining, cells were fixed with BD Cytofix/Cytoperm™ (554722, BD Biosciences) followed by antibody incubation in BD Perm/Wash™ Buffer (554723, BD Biosciences). After staining, the cells were washed twice and resuspended in 150 μl FACS buffer mixed with 15 μl CountBright beads (C36950, Invitrogen). Samples were recorded on an LSR II flow cytometer (BD Biosciences) and analyzed using FlowJo (Version 9.9, Tree Star). For sorting of GC B cells from the PPs and spleen, total cells or splenocytes were stained with a cocktail of fluorophore-conjugated antibodies before being sorted on a FACSAria cell sorter (BD Biosciences).

Seahorse flux analyzer studies

Naïve B cells were isolated from spleens of specified genotypes by CD43 bead-based negative selection. To prepare the cell culture plates (101085–004, Agilent) for the assay, Cell-Tak (354240, Corning) was diluted to ~23 μg ml^{-1} in 2 ml 0.1 M $NaHCO_3$ at pH 8.0 and 20 μl of the solution is pipetted into each well. After 20 min, the solution was aspirated, and the wells were washed with 100 μl distilled water. After the plates were air-dried, 1×10^6 cells were resuspended in 40 μl of Seahorse minimal media and transferred into each well. Cells were spun at 300*g* for 1 min to allow them to stick to the wells. Both naïve and activated cells were resuspended in Seahorse minimal media and supplemented with glutamine (Glyco stress test) or glutamine, pyruvate and glucose (Mito stress test). All the inhibitors provided in the kit were resuspended according to the manufacturer's instructions (103010-100 and 103020-100, Agilent). After about 30–40 min of incubation in a non-CO_2 incubator, the plates were loaded into an XF96 Seahorse analyzer for ECAR and OCR measurements.

ELISA

Assays were done in clear, flat-bottom, 96-well MaxiSorp plates (439454, Thermo Fisher Scientific). Coating antibodies for binding IgM, IgG1, IgG2b, IgG2c, IgG3 and IgA (1020–01, 1070–01, 1090–01, 1079–01, 1100–01 and 1040–01, respectively, SouthernBiotech) were used at 3 μg ml^{-1} in PBS at a pH of 8.0. Each plate was coated with antibody overnight at 4 °C (100 μl per well). Plates were washed 4× with 0.05% PBST and blocked thereafter with an ELISgA diluent (00–4202-56, eBioscience) for 3 h at 25 °C or overnight at 4 °C (250 μl blocking buffer per well). Plates were washed 3×, loaded with serum samples and standards (100 μl per well) and incubated for 2.5 h at 25 °C or overnight at 4 °C. The following isotype standards were used to calculate absolute concentration values: IgM (14– 4752-81, eBioscience), IgG1 (0102–01, SouthernBiotech), IgG2b (14–4732-81, eBioscience), IgG2c (0122–01, SouthernBiotech), IgG3 (553486, BD Pharmingen) and IgA (553478, BD Pharmingen). Plates were washed 5–6× and secondary antibodies for detecting IgM, IgG1, IgG2b, IgG2c, IgG3 and IgA (1020–05, 1070–05, 1090–05, 1079–05, 1100–05 and 1040–05, respectively, SouthernBiotech) were used at a 1:2,000 dilution for 1.5 h at 25 °C (100 μl per well). After 6–7 washes, 100 μl of TMB substrate (00–4201-56, eBioscience) was added to each well to develop for 30–60 s, and 1 M phosphoric acid was used to stop the reaction. Plates were read at 450 nm on a BioTek Synergy HT detector. Absolute concentrations of serum antibodies were determined by interpolation from the standard curve; the sample values were kept within standard and linear ranges. All samples were analyzed in triplicate over a six-step dilution series. An eleven-step standard curve was generated for each plate. For NP-specific assays, plates were coated with 9 μg ml^{-1} NP (8)-BSA (N-5050L-10, Biosearch Technologies) or NP (30)-BSA (N-5050H-10, Biosearch Technologies) dissolved in borate buffered saline (100 mM boric acid, 25 mM sodium borate, pH 8.2, 75 mM NaCl). Relative titers were determined by interpolation on the plate reference curve, generated for each plate using a constant sample, with attention paid to keeping within the plate reference and sample linear ranges. All samples were done in duplicate over a six-step dilution series.

In vivo BrdU labeling

For cell-cycle analysis, BrdU included in the FITC BrdU Flow kit (559619, BD Biosciences) was injected intraperitoneally at 1 mg per kg of body weight 1 h before euthanasia. Splenocytes were harvested and stained with viability dye and antibodies against surface proteins. Following that, the cells were fixed according to the manufacturer's guidelines, treated with DNase for 1 h at 37 °C, and stained intracellularly with FITC-conjugated anti-BrdU antibody for 20 min. Before analysis, cells were counterstained with 7-AAD for total DNA content quantification.

Immunoblotting

Frozen cell pellets were resuspended in 2× Laemmli buffer (1610737, Bio-Rad) supplemented with β-mercaptoethanol. The lysate was incubated at 95 °C for 5 min and then sonicated thrice for 10 s at 30% amplitude using a Branson digital sonicator. After sonication, the lysate was spun at 15,000*g* for 5 mins and analyzed for protein concentration by Bradford assay (5000001, Bio-Rad). Lysates were run on 12% SDS–PAGE gels and

the resolved proteins were transferred at 19 V onto an Immobilon PVDF membrane (05317–10EA, Millipore). The blots were blocked with 5% non-fat milk and incubated with the primary and secondary antibodies as indicated.

Immunofluorescence

Spleen sections of immunized mice were dissected, immediately embedded in Tissue-Tek OCT Compound (4583, Sakura Finetek USA) and flash frozen in dry ice and fixed with 4% paraformaldehyde. The tissues were then sliced into 6-mm sections and stained with appropriate primary and secondary antibodies. Primary antibodies used were anti-IgD (1120–01, Southern Biotech), PNA-biotin (B-1075, Vector Laboratories) and anti-B220 (ab64100, Abcam). Secondary antibodies used were donkey anti-rat Alexa Fluor 488 (A21208, Invitrogen; 1:5,000 dilution), donkey anti-rat Alexa Fluor 594 (A21209, Invitrogen; 1:5,000 dilution) and cyanine 5–conjugated streptavidin (Jackson ImmunoResearch Laboratories; 1:5,000 dilution). The nuclei were counterstained with DAPI (Boehringer Mannheim). Sections were mounted with FluorSave (Calbiochem). For scanning of the slides, a 20×/0.8 NA objective was used on a Panoramic flash (3D Histech) with regions of interest drawn manually using CaseViewer (3D Histech). Raw, unedited images were imported as TIFF files and then analyzed with ImageJ/FIJI. Adobe P-S6 was used for formatting images and making panels.

Real-time PCR

Total RNA from naïve and activated B cells and heart muscle homogenate were isolated using Quick-RNA Microprep Kit (R1050, ZymoResearch). High-Capacity cDNA Reverse Transcription Kit (4368814, Applied Biosystems) was then used to synthesize cDNA from the purified total RNA. Amplification of the cDNA transcripts was performed using TaqMan Fast Advanced Master Mix (4444557, Applied Biosystems) and Taqman probes specific for *Ldha* (Mm01203357_g1) and *Ldhb* (Mm01267402_m1). Quantitative PCR experiments were conducted in a 384-well format using an Applied Biosystems QuantStudio 6 Flex instrument. Relative gene expression was calculated and plotted as $-\Delta C_T$ wherein *Ubc* served as the housekeeping control.

T_{FH}–B cell co-culture assay

T_{FH}-B cell co-culture assay was performed as previously described[56]. Mice were immunized intraperitoneally and in both hind footpads with 50 μg of NP-CGG emulsified in Alum. After boosting on d10, the mice were euthanized at d14 and spleens dissected. On day 14, a single-cell suspension was prepared from the spleen and draining lymph nodes (inguinal and popliteal) by mechanical dissociation, and were lysed with ACK lysis buffer. $CD4^+$ T cells were isolated using CD4 MicroBeads (130–117-043, Miltenyi Biotec) according to the manufacturer's instructions, and T_{FH} cells ($CD4^+CD19^-TCRb^+$ $CXCR5^+PD\text{-}1^+$ $GITR^-$) were subsequently sorted from the enriched $CD4^+$ T cells. Wild-type B cells were isolated from the flow-through of $CD4^+$ T cell isolation using CD19 MicroBeads (130–121-301, Miltenyi Biotec) according to the manufacturer's instructions, followed by sorting of $CD19^+CD4^-$ cells. Around 5×10^5 wild-type B cells and 3×10^5 *Ldha*-sufficient or -deficient T_{FH} cells were co-cultured in a 96-well round-bottom plate in 200 μl complete RPMI media in the presence of 30 μg ml^{-1} NP-CGG for 6 d. IgG1 in the supernatant

was measured by ELISA, and the cells were stained for B220, MHC-II, GL7, IgG1 and Ki67 using the Foxp3/Transcription Factor Staining Buffer Set (00–5523-00, Thermo Fisher Scientific).

Bulk RNA-sequencing

Total RNA was extracted from LDHA-sufficient and -deficient cells via standard TRIzol™ extraction (15596026, Thermo Fisher Scientific). Libraries were generated and sequenced on a NovaSeq platform by MSKCC Integrated Genomics Operation. RNA sequencing data was aligned with STAR v2.7.7a (Dobrin) to the mm10 genome and annotated using GATK v4.1.9.0 (Van der Auwera). Counts were generated using featureCounts v2.0.1 (Liao), normalized to transcripts per million via a custom pipeline in R v4.2.1 and visualized using ggplot2 v2.3.4.0.

scRNA-seq and 10x Genomics gene expression analysis

Ldha$^{fl/fl}$*Cd23*^{Cre} and control mice were immunized with NP-CGG and cells harvested from the spleen at d4. For scRNA-seq, total splenocytes were stained with antibodies targeting surface proteins. For scRNA-seq downstream processing, the cells from each mouse were stained individually with a single TotalSeq-C barcoded antibody (C0305–C0310, BioLegend). After staining the activated cells (GL7^{+}) and non-activated cells (GL7^{-}) were sorted with a BD FACSAria (BD Biosciences) and collected in a low-binding microcentrifuge tube containing PBS + 1% BSA. The tubes were deposited at the Single Cell Research Initiative, a genomics core facility dedicated to single-cell sequencing at MSKCC, for 10x V(D)J sequencing.

The V(D)J data were processed using the Cell Ranger v6.0.2 vdj pipeline, and the aggregated output from all the cells was analyzed with the Immcantation suite toolbox v4.3.0 (http://immcantation.org/). V(D)J assignment, based on the mouse IMGT and IgBLAST reference databases, was carried out using the Change-O tool. Cells with non-productive V–J heavy chain spanning pairs were removed. The mutational load was quantified with the SHazaM Immcantation package and the observedMutations function was applied to the entire heavy chain sequence. The AddMetaData Seurat function was used to integrate the SHM and BCR isotype data into the Seurat object (see below).

The gene expression and hashtag matrices, generated by the Cell Ranger v6.0.2 pipeline, were processed via Seurat v4.2.0 in R v4.2.1. The hashtag matrix was intersected with the gene matrix to include only barcoded cells. Cells were then classified according to a 0.99 positive quantile using HTODemux. We removed doublets, and after standard cell filtration, we retained 1,814 cells and used the 2,000 most variable genes for clustering. Excluding the monocytes (as defined by clustering) from further analysis yielded 1,788 cells across all six mice. The top nine principal components were used for unsupervised clustering, and the data were visualized in two-dimensional space using UMAP. The BCR data described in the V(D)J sequencing analysis were overlaid onto these cells, and the 1,065 (59.6%) B cells with well-defined BCRs were retained for BCR mapping and analysis.

J_H4 intronic sequence amplification and analysis

GC B cells were sorted from the spleen of NP-CGG-immunized mice at d14. Genomic DNA was harvested using the DNeasy Blood & Tissue Kit (QIAGEN) according to the manufacturer's protocol, except for the elution step in which the DNA on the spin column was eluted in 50 μl of elution buffer. The reverse complement primer probes (RC-probes) targeting the J_H4 intron (Fwd: 5′-CATAACAAAGGTTAAAAATAAAGAC-3′; Rev: 5′-GCCTGACATCTGAGGACTC-3′) were synthesized by Nima-Gen and used for the generation of indexed amplicons by reverse complementary PCR (RC–PCR). The addition of Illumina universal indexes and sequence adaptors to the J_H4-specfic RC-probes and the amplification of the exonic and intronic sequences with these RC-generated region-specific indexing primers were performed in a probe-polymerase mix. The mix was composed of (1) RC–PCR HiFi Master Mix, (2) RC-probe mix, (3) RC–PCR probe dilution buffer (all from NimaGen), and (4) 80 to 100 ng of genomic DNA. The following thermocycling program was used: (1) 98 °C for 2 min; (2) 98 °C for 10 s, 58 °C for 10 min at a ramp rate of 0.1 °C/s and 72 °C for 1 min; (3) 98 °C for 10 s, 80 °C for 1 s, 58 °C for 1 h and 30 min at a ramp rate of 0.1 °C/s and 72 °C; (4) go to step 3 once; (5) 98 °C for 10 s, 80 °C for 1 s, 58 °C for 2 min at a ramp rate of 0.5 °C/s and 72 °C for 1 min; (6) go to step 5 33 times; and (6) 4 °C hold. PCR amplicons were purified using Agencourt AMPure XP beads (Beckman Coulter) and resuspended in 50 μl of Tris-EDTA buffer. Indexed amplicons were sequenced on a NovaSeq platform, and an average of 10 to 20 million 150-bp paired-end reads were generated for each sample (MSKCC Integrated Genomics Operations). Paired-end fastq files were demultiplexed and recombined into discrete samples. Each sample was processed according to the following pipeline: (1) GATK v4.1.9.0 to convert to SAM format and to remove adaptors and low-quality bases; (2) bbmap v38.93 to clump duplicate reads into clusters (6 passes, 0 substitutions allowed); (3) grep to include only clusters with at least 100 reads (utilizing the V(D) J recombination as a cellular barcode); (4) bbmap v38.93 to align to a custom JH4 reference genome (see below); (5) GATK v4.1.9.0 to convert back to fastq format; (6) realignment with bbmap v38.93; and (7) GATK v4.1.9.0 to remove read groups allowing for pileup into a unique text file. Pileup output was processed in R v4.2.1. Each position in the reference genome (V1–64:D3–1:J4:J4_intron) was run separately via a custom script in R v4.2.1. In particular, the nucleotides aligning to positions 1,100–1,139, excluding 1,108, were compared to the reference and the total counts of correct reads and coverage at the associated position were placed into a combined data frame. The total fraction of correct bases read for each sample was then compared between samples in ggplot2 (v2.3.4.0).

LDHA genotyping

Primers:

LDHA-1: 5′-GCAGGAGCTGATTTCACACA

LDHA-3: 5′-CCAACACCCAGGAAGATTGT

LDHA-9: 5′-GGACAGCTGATCCAGAGAGC

The PCR products were run on a 2% agarose gel to resolve the bands. Wild type allele, 195 bp; floxed allele, 384 bp; null (deleted) allele, 483 bp.

Data and statistical analysis

Results are presented as mean ± s.e.m., mean ± s.d., and mean only wherever applicable. *P* values were calculated by unpaired, two-tailed *t*-test or by two-way ANOVA with $*P \leq 0.05$, $**P \leq 0.01$, $***P \leq 0.001$, $****P \leq 0.0001$. All data were assumed to come from normal distributions. Control animals in which immunization had failed or assay values that fell below the detection limit were excluded from analysis. Data collection and analysis were not performed blind to the conditions of the experiments. No statistical methods were used to predetermine sample sizes but our sample sizes are similar to those reported in previous publications from our laboratory[57,58].

Reporting summary

Further information on research design is available in the Nature Portfolio Reporting Summary linked to this article.

Extended Data

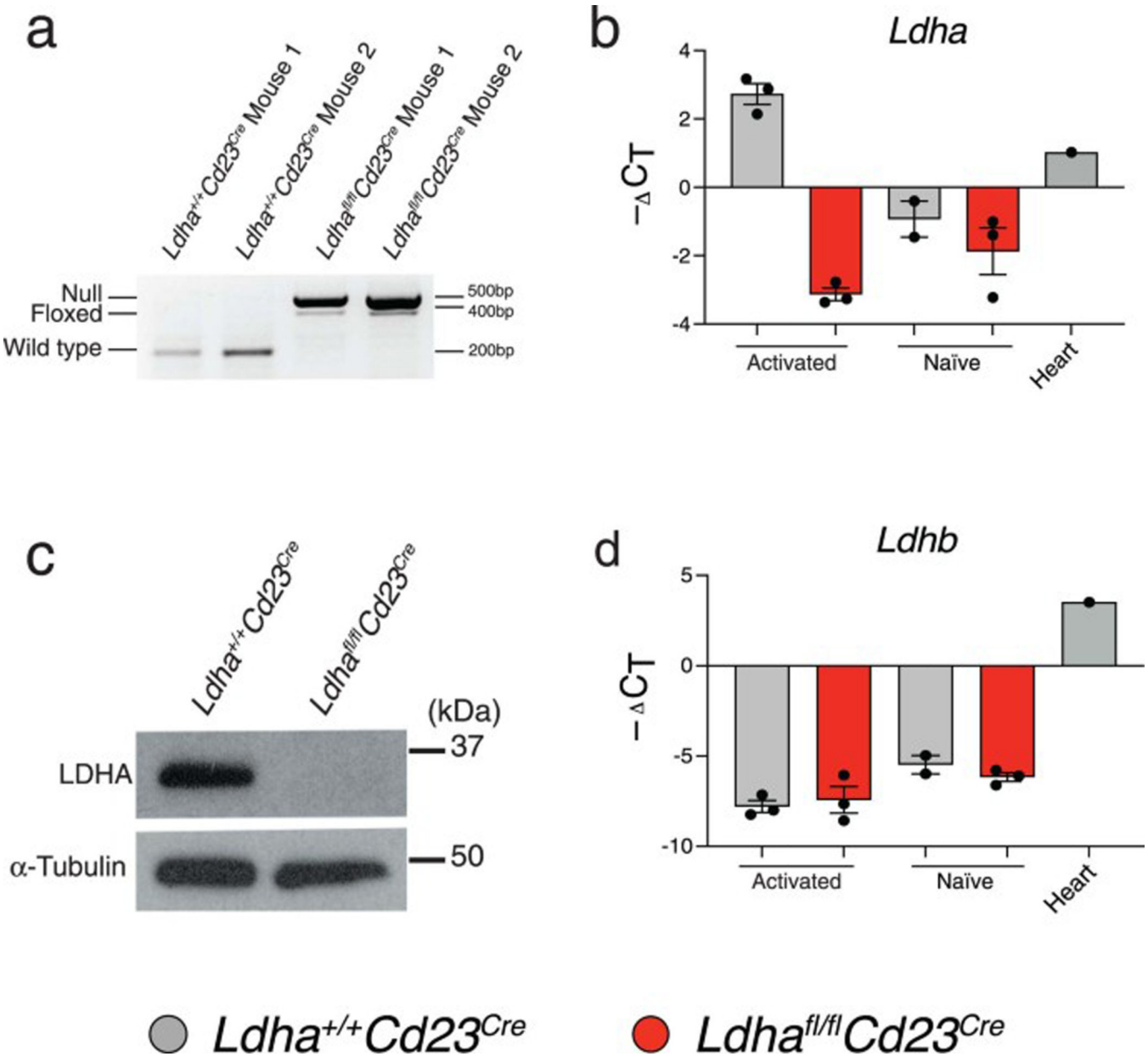

Extended Data Fig. 1 |. Confirmation of *Ldha* deletion in naïve B cells.

a, PCR analysis of genomic DNA from naïve splenic B cells. Two $Ldha^{fl/fl}Cd23^{Cre}$ and two $Ldha^{+/+}Cd23^{Cre}$ control mice were analyzed for the presence of the deleted (null), floxed and wild type *Ldha* alleles. Data is representative of 3 independent experiments. **b**, Naïve splenic B cells harvested from mice of the indicated genotypes ($n = 2$ for $Ldha^{+/+}Cd23^{Cre}$, $n = 3$ for $Ldha^{fl/fl}Cd23^{Cre}$) or splenic B cells activated with LPS + IL-4 for 48 h ($n = 3$ for each group) were examined for expression of *Ldha* by qPCR. Heart tissue harvested from $Ldha^{+/+}Cd23^{Cre}$ mice ($n = 1$) was used as a control. **c**, Naïve splenic B cells were activated *ex vivo* with LPS + IL-4 for 72 h and whole cell protein extracts were

analyzed by immunoblotting using antibodies against LDHA or α-tubulin (control). Data is representative of three independent experiments. **d**, Naïve and activated B cells were analyzed for expression of *Ldhb* by qPCR. $n = 3$ for each group, except $n = 2$ for naive $Ldha^{+/+}Cd23^{Cre}$ B cells and $n = 1$ for heart tissue. For panels **b** and **d**, data represents mean ± s.d.

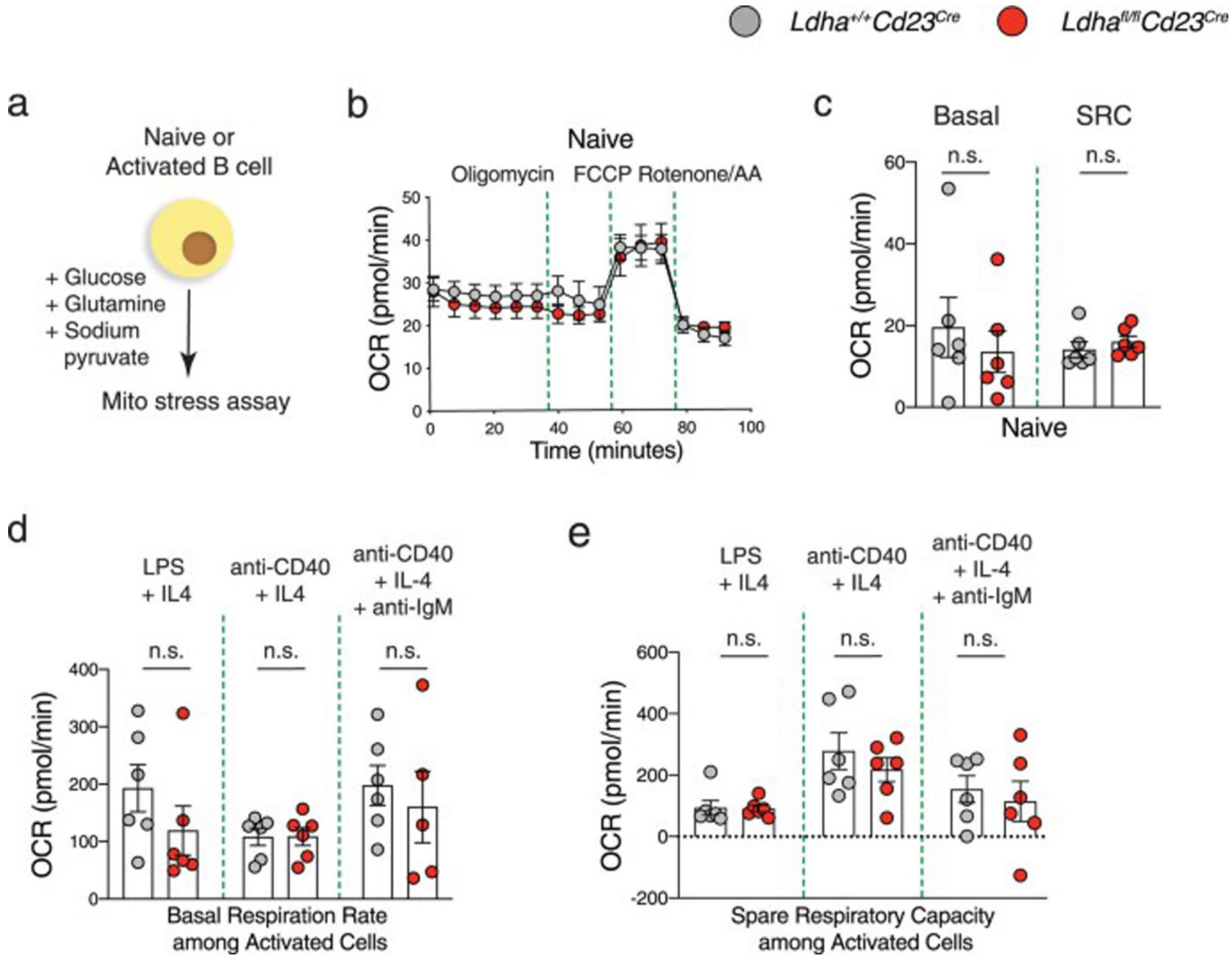

Extended Data Fig. 2 |. LDHA governs aerobic glycolysis in B cells.

a, Schematic representation of mito stress assays performed in a Seahorse analyzer. The mito stress assay measures the oxygen flux of cells cultured in glucose-sufficient media supplemented with glutamine and sodium pyruvate. During this assay, the oxygen consumption rate (OCR) is first measured at baseline and after the sequential addition of oligomycin (which inhibits ATP synthase and reduces OCR), FCCP (an uncoupling agent that disrupts the mitochondrial membrane potential without inhibiting the electron transport chain and allows oxygen consumption to reach a maximum), and a mixture of rotenone and antimycin A (AA) (which shuts down mitochondrial respiration). **b**, Representative graph of OCR of naïve B cells at baseline and following the indicated perturbations. **c**,

Quantification of OCR and of spare respiratory capacity (SRC) of naïve splenic B cells from *Ldha*$^{fl/fl}$*Cd23*^{Cre} and *Ldha*$^{+/+}$*Cd23*^{Cre} (control) mice. SRC was calculated as the difference of FCCP-stimulated maximum OCR and basal OCR. **d**, **e**, Naïve splenic B cells were activated with LPS + IL4, anti-CD40 + IL4 or anti-CD40 + IL4+anti-IgM for 48 h and OCR and SRC was quantified. *p* values were calculated using unpaired, two-tailed *t*-tests. For panels **b**–**e**, *n* = 6 for each indicated genotype and representative of three independent experiments. Data points and bars represent mean ± s.e.m.

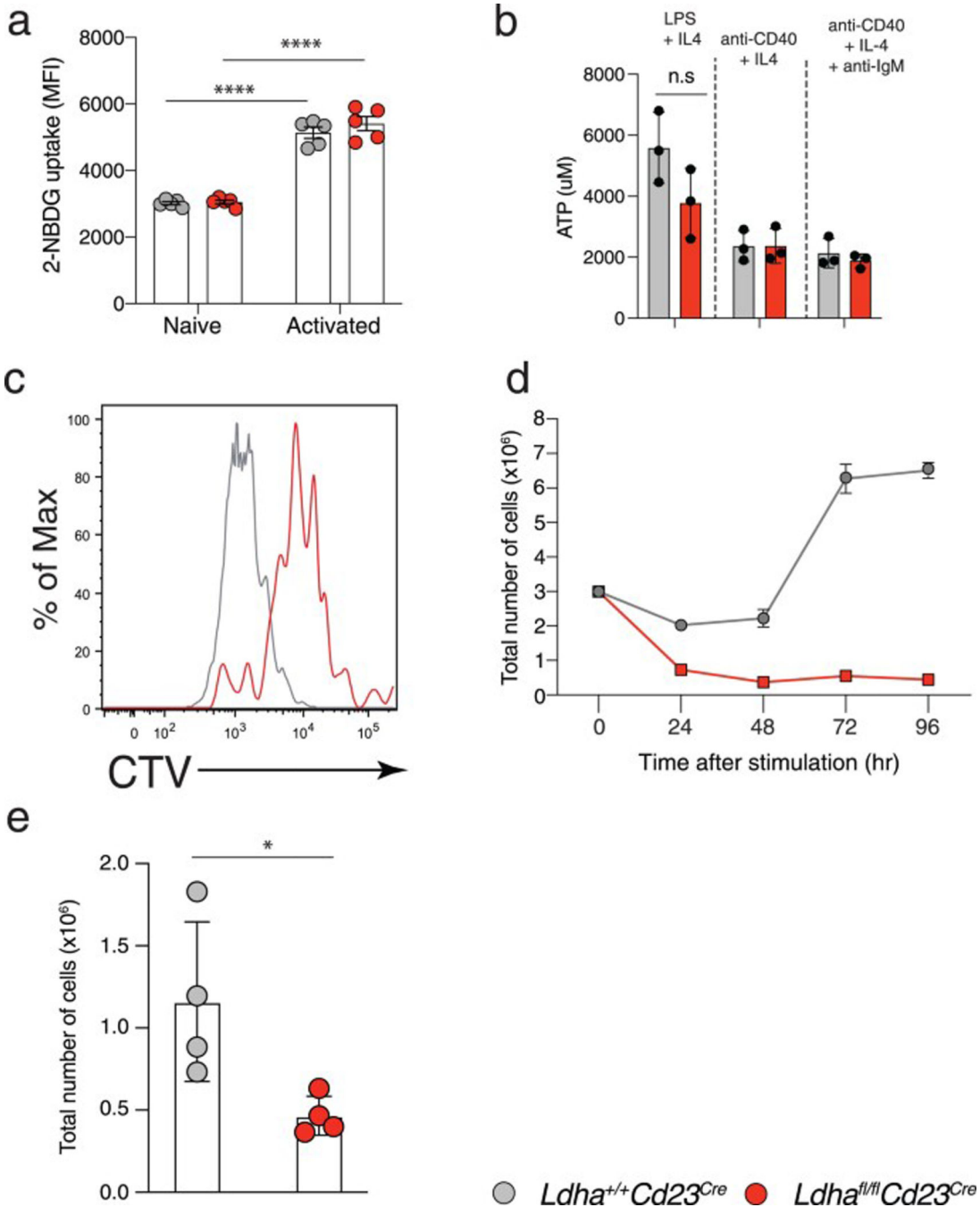

Extended Data Fig. 3 |. Cellular homeostasis in LDHA-deficient activated B cells.
a, Uptake of the fluorescent glucose analog 2-NBDG. Naïve B cells (n = 5 for each genotype) were activated *ex vivo* with LPS + IL4 for 48 h, incubated with 11 mM of 2-NBDG for 15 min, and 2-NBDG uptake was quantified by flow cytometry. Data is representative of two independent experiments. **b**, Splenic B cells from $Ldha^{fl/fl}Cd23^{Cre}$ (n = 3) and $Ldha^{+/+}Cd23^{Cre}$ (control, n = 3) mice were activated *ex vivo* as indicated for 48 h and intracellular ATP level was determined. Data is representative of two independent experiments. **c**, **d**, Splenic B cells from $Ldha^{fl/fl}Cd23^{Cre}$ and $Ldha^{+/+}Cd23^{Cre}$ (control) mice were labeled with Cell Trace Violet (CTV) dye, activated *ex vivo* for 48 h with LPS + IL4, and CTV dilution was determined by flow cytometry as a measure of cell proliferation. Data shown is representative of three independent experiments. **d**, Splenic B cells (1×10^6) were harvested from mice of the indicated genotypes (n = 7 for each group), stimulated with LPS + IL-4 and cell numbers were quantified at the indicated time points. **e**, Splenic B cells (1×10^6) harvested from mice of the indicated genotypes (n = 4 for each group) were stimulated with LPS + TGFβ + anti-IgD *ex vivo* and cell numbers were determined at 96 h post-activation. Data is representative of two independent experiments. Bars represent mean ± s.e.m. *$p \leq 0.05$, ****$p \leq 0.0001$ by unpaired, two-tailed t-test.

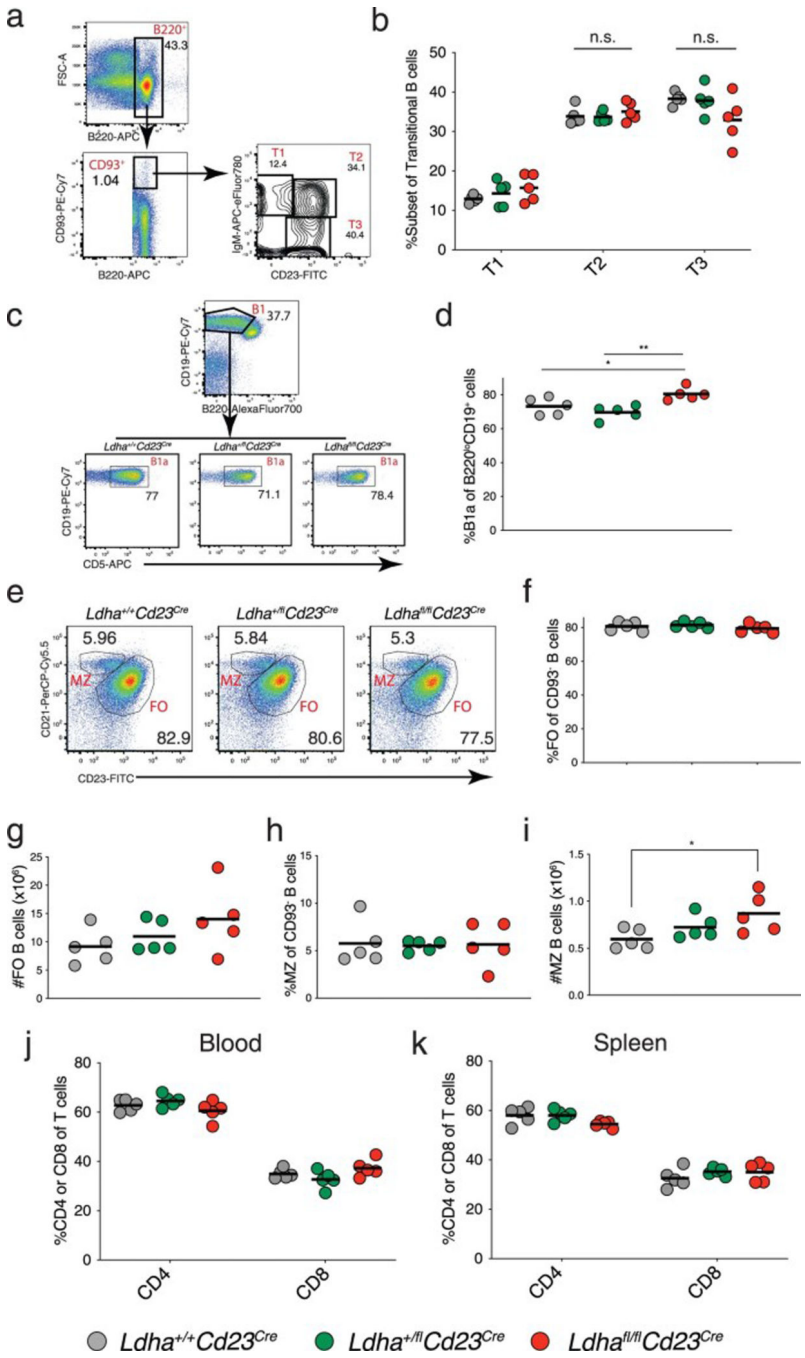

Extended Data Fig. 4 |. B cell subsets at homeostasis.

a, Representative flow plot of splenic transitional T1 ($B220^{+}CD93^{+}CD23^{-}IgM^{hi}$), T2 ($B220^{+}CD93^{+}CD23^{+}IgM^{hi}$) and T3 ($B220^{+}CD93^{+}CD23^{+}IgM^{low}$) B cells. Live singlets from the spleen were first gated for $B220^{+}CD93^{+}$ cells and then gated for surface expression of IgM and CD23 as indicated. **b**, Quantification of T1, T2, and T3 B cells in the spleens of mice of indicated genotypes. **c**, Representative flow plots of B1a ($B220^{low}CD19^{+}CD5^{+}$) B cells in the peritoneum of mice. Live singlets from the peritoneal cavity were first gated for $B220^{low}CD19^{+}$cells and then gated for surface expression of $CD5^{2}$. **d**, Quantification

of B1a cells in the peritoneum of mice of the indicated genotypes. **e**, Representative flow plots of marginal zone (MZ) B cells and follicular zone (FO) B cell subsets in the spleen of mice of the indicated genotypes. Live singlets from the spleen were first gated for mature $B220^{+}CD93^{-}$B cells and then analyzed for surface expression of CD21 and CD23. **f**,**g**, Frequency and absolute number of FO B cells. **h**, **i**, Frequency and absolute number of MZ B cells. **j**, Frequency of $CD4^{+}$ and $CD8^{+}$ T cells (among live singlets) in peripheral blood and **k**, in the spleen of mice of the indicated genotypes. Each datapoint represents a single mouse. Bars represent mean. $*p \leq 0.05$, $**p \leq 0.01$, p-values were calculated using unpaired, two-tailed *t*-test. For panels **b**, **d**, **f**–**k**, $n = 5$ of each genotype and data is representative of two independent experiments.

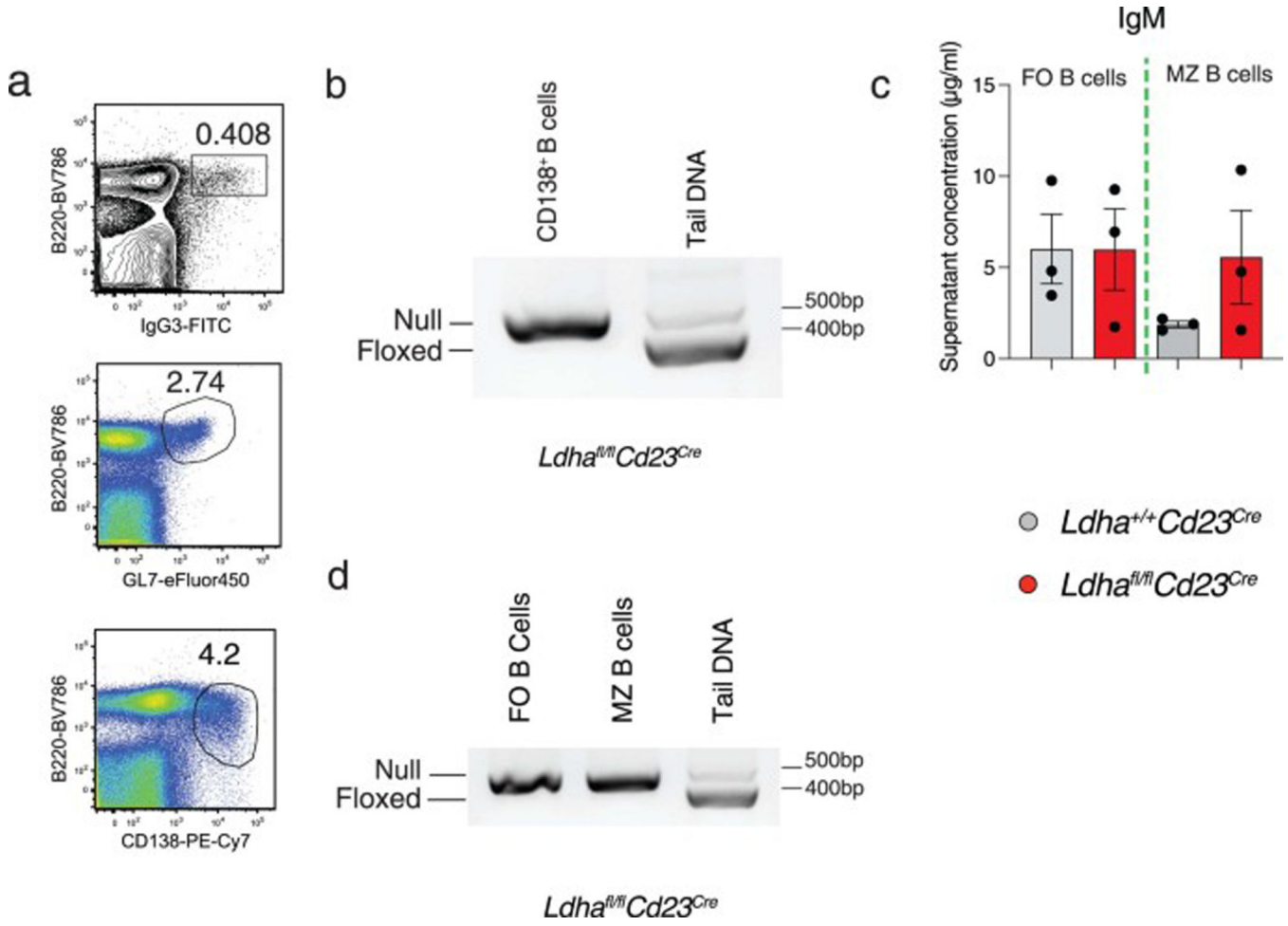

Extended Data Fig. 5 |. Confirmation of *Ldha* deletion in CD138+ plasmablasts, marginal zone (MZ) and follicular (FO) B cells; IgM ELISA of culture supernatants of ex vivo FO and MZ B cells.

a, Gating strategy for the analysis of $B220^{lo}$ $CD138^{+}$ cells in the spleens of mice challenged with LPS. **b**, Representative PCR showing the genomic deletion of the floxed *Ldha* exon in $CD138^{+}$ plasmablasts sorted from the spleens of $Ldha^{fl/fl}Cd23^{Cre}$ and control mice at d5 after LPS challenge. Tail DNA was used as a control to detect both the null and floxed alleles. Image of ethidium bromide-stained gel shown is representative of three independent

experiments. **c**, Purified FO or MZ B cells of the indicated genotypes ($n = 3$) were cultured *ex vivo* for 72 h with LPS + IL4 or LPS respectively and IgM concentration in the culture supernatants was determined by ELISA. Bars represent mean ± s.e.m. **d**, Representative PCR depicting genomic deletion of *Ldha* from sorted FO and MZ B cells cultured with LPS. Image of ethidium bromide-stained gel shown is representative of three independent experiments.

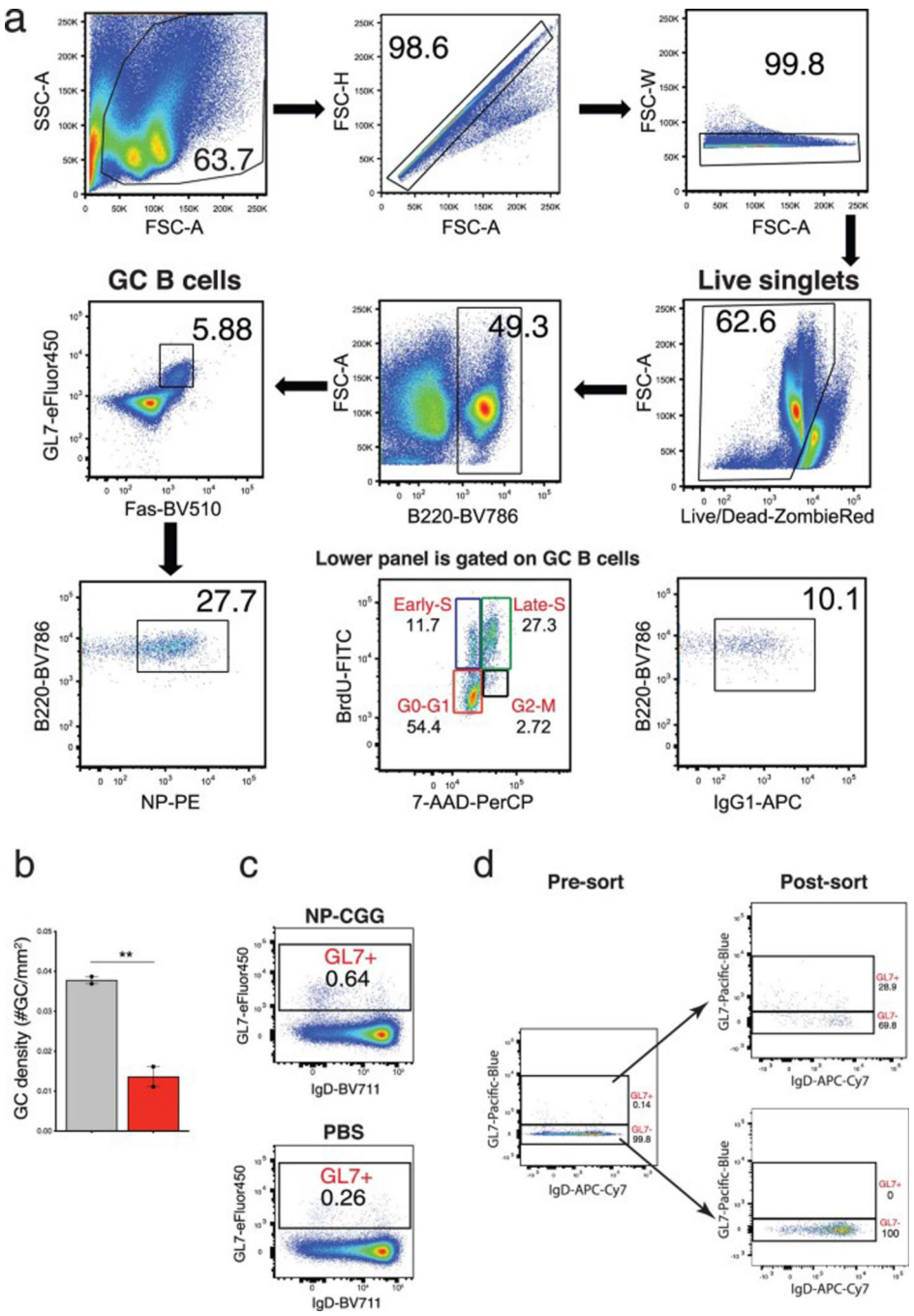

Extended Data Fig. 6 |. Gating strategy for analysis of GC B cells following NP-CGG immunization, quantification of GC density and gating strategy for sorting of GL7$^+$ and GL7$^-$ B cells.

a, Gating strategy for analysis of GC B cells and associated populations in the spleens of NP-CGG immunized mice. **b**, Mice were immunized intraperitoneally with NP-CGG, boosted at d10 and the GC density in the spleen sections from *Ldha*$^{+/+}$ *Cd23*^{Cre} (grey bar) and *Ldha*$^{fl/fl}$ *Cd23*^{Cre} (red bar) mice was quantified at d14 post-immunization. Each data point represents one independent experiment in which data from the spleen sections of 3 mice per genotype were pooled. Data presented is mean ± s.e.m. **c**, Detection of pre-GC B cells. Wild type mice were immunized intraperitoneally with NP-CGG or with PBS and the frequency of GL7$^+$ cells quantified at d4 post-immunization. **d**, Gating strategy for the sorting of GL7$^+$ and GL7$^-$ cells from the spleens of NP-CGG immunized mice at d4 post-immunization. Sorted GL7$^+$ and GL7$^-$ cells were mixed 3:1 and subjected to scRNA sequencing analysis. Flow cytometry of the post-sort cells is shown.

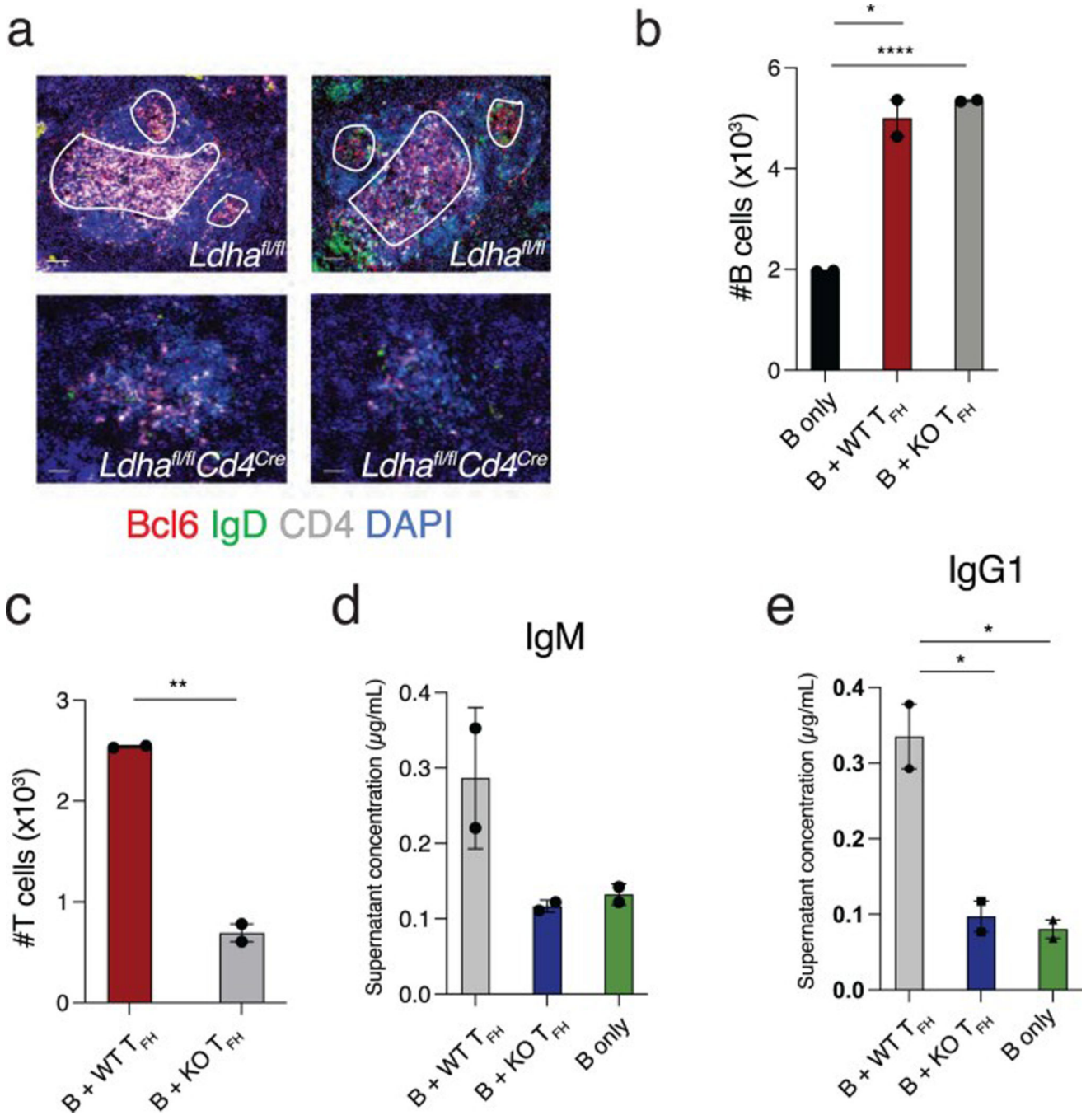

Extended Data Fig. 7 |. LDHA in T cells regulates GC B cell responses.

Ldha$^{fl/fl}$ and *Ldha*$^{fl/fl}$*Cd4*^{Cre} mice were immunized intraperitoneally with NP-CGG, boosted at d10, and analyzed at d14. **a**, Immunofluorescence staining of frozen spleen sections harvested at d14. Image is representative of $n = 3$ mice per genotype. Scale bar represents 50 μm. **b**–**e**, Splenic B cells (5×10^5) from wild type mice were co-cultured with T_{FH} cells (3×10^5) purified from *Ldha*$^{fl/fl}$*Cd4*^{Cre} ($n = 2$ pooled samples) or *Ldha*$^{fl/fl}$ ($n = 2$ pooled samples) control mice. The cells were analyzed at d6 post initiation of culture. **b**, **c**, Number of B and T_{FH} cells at d6. **d**, **e**, Antibody titers of IgM and IgG1 in culture supernatant. *p ≤ 0.05, by

unpaired, two-tailed *t*-test. Data represents two biological samples, each pooled from 4 mice per genotype. Bars represent either mean ± s.e.m (panels **b**, **c**, and **e**) or mean ± s.d. (panel **d**).

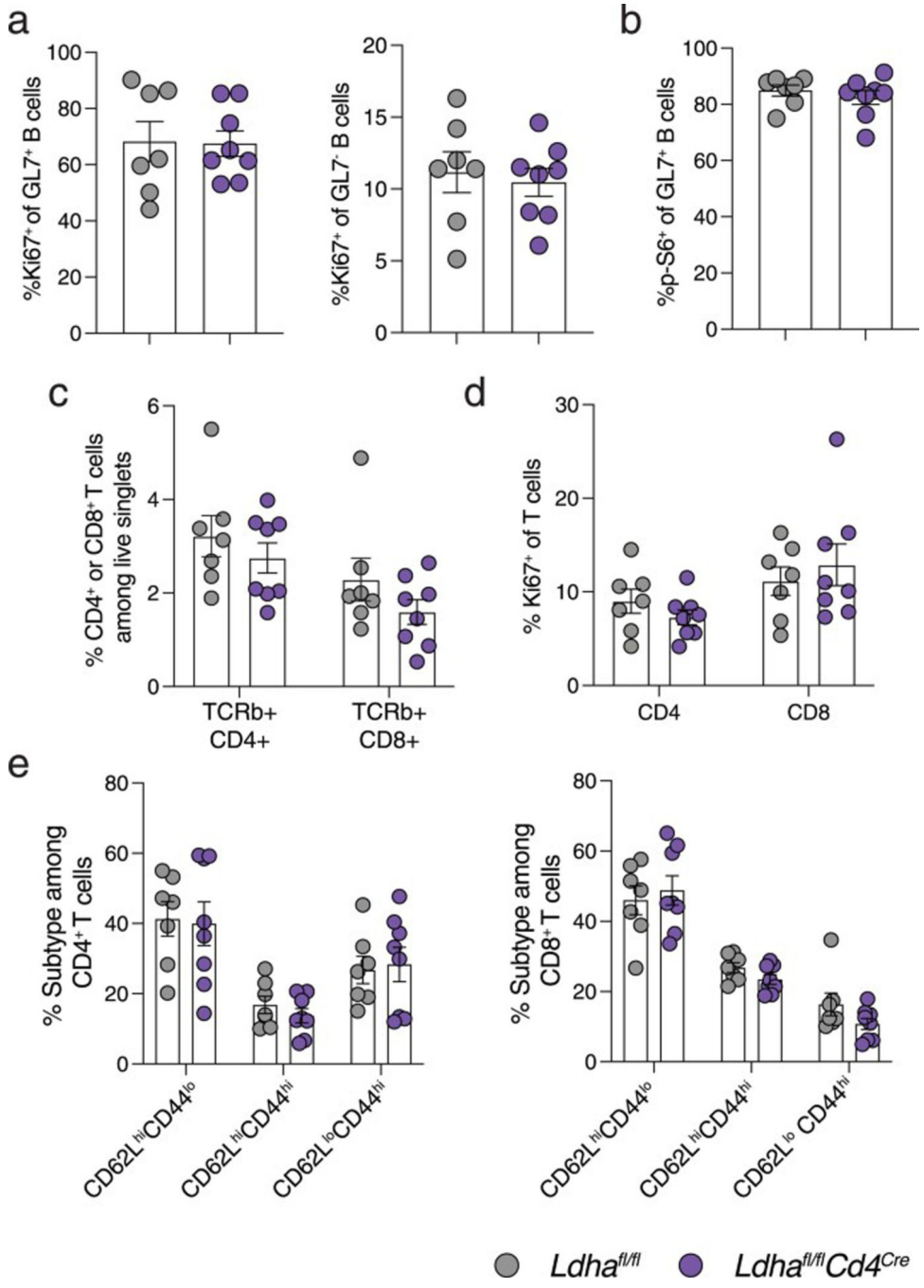

Extended Data Fig. 8 |. LDHA in T cells is dispensable for LPS-dependent extrafollicular responses.

The spleen of *Ldha*$^{fl/fl}$*Cd4*^{Cre} ($n = 8$) and *Ldha*$^{fl/fl}$ (control, $n = 7$) mice were analyzed at d5 after LPS administration. **a**, Staining of Ki67 in activated (GL7^{+}) and unactivated (GL7^{-}) B cells in mice of indicated genotypes. **b**, mTORC1 activity was quantified from the frequency

of phosphorylated S6 (p-S6) positive cells in activated ($GL7^+$) B cells. **c**, Frequency of $CD4^+$ and $CD8^+$ T cells among live singlets. **d**, Ki67 staining of $CD4^+$ and $CD8^+$ T cells. **e**, Quantification of naïve ($CD62L^{hi}CD44^{lo}$), central memory ($CD62L^{hi}CD44^{hi}$) and effector ($CD62L^{lo}CD44^{hi}$) $CD4^+$ and $CD8^+$ T cells at d5 post-LPS challenge. Data is representative of three independent experiments. Bars represent mean ± s.e.m.

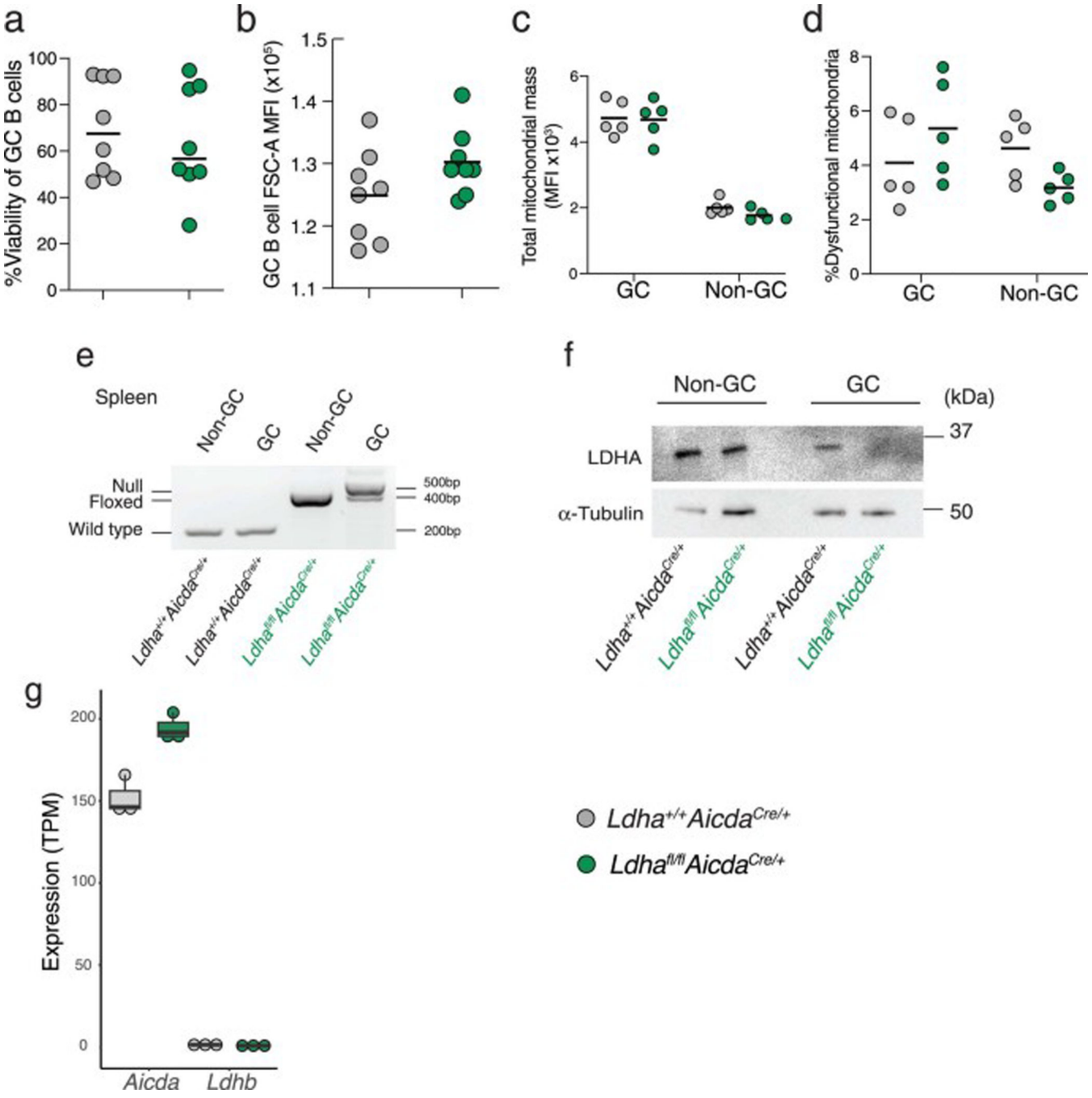

Extended Data Fig. 9 |. *Ldha*$^{fl/fl}$*Aicda*$^{Cre/+}$ mice can mount a robust GC response.

Ldha$^{fl/fl}$*Aicda*$^{Cre/+}$ and *Ldha*$^{+/+}$*Aicda*$^{Cre/+}$ (control) mice were immunized intraperitoneally with NP-CGG, boosted at d10, and analyzed at d14. **a**, Viability of GC B cells as measured by cells negative for Zombie Red viability dye. **b**, Cell size of viable GC B cells as measured by quantifying the MFI of forward scatter (FSA). **c**, Mitochondrial mass was quantified by measuring the MFI of MitoTracker™ Green FM Dye among the GC and non-GC B cells. **d**, Frequency of dysfunctional mitochondria was measured by quantifying the fraction of live GC and non-GC B cells negative for MitoTracker™ Red CMXRos. **e**, PCR of genomic DNA of GC and non-GC B cells sorted from spleens of mice of the indicated genotypes. **f**, Immunoblotting of whole cell extracts prepared from GC and non-GC B cells sorted from the Peyer's patches and spleens of mice of the indicated genotypes to detect LDHA and α-tubulin (control) proteins. **g**, Expression of *Ldha* and *Ldhb* in sorted GC B cells. Bars represent mean. Each datapoint represents a single mouse ($n = 3$). The box plot depicts the first quartile, third quartile, and the median of the dataset. Values that fall within 1.5 times the interquartile range above the third quartile and below the first quartile are represented by the whiskers. The gating strategy for the sorting of GC B cells is the same as that in Extended Data Fig. 6a. For panels **a** and **b**, $n = 8$ for each genotype; data is representative of two independent experiments. For panels **c** and **d**, $n = 5$ for each genotype and data is representative of two independent experiments. For panels **e**, and **f**, data is representative of 2 independent experiments with 3 to 5 mice per experiment.

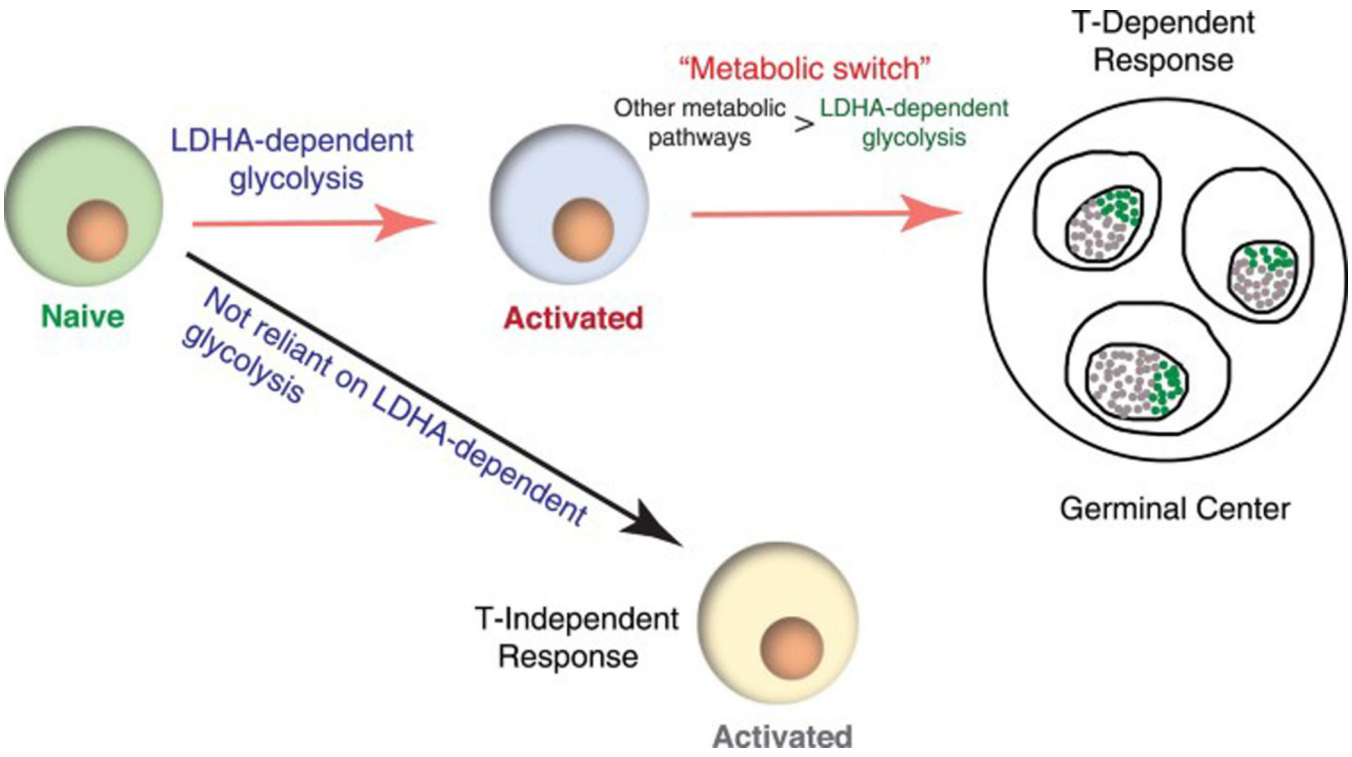

Extended Data Fig. 10 |. Working model depicting metabolic requirements in naïve and in activated B cells.

Proposed model suggesting different metabolic constraints in B cells committed to either a T-dependent or a T-independent pathway for an optimal humoral response. LDHA-mediated glycolysis is essential for the early activation of B cells during a T-dependent GC response

but is largely dispensable once the activated B cells are fully engaged in a GC reaction (‘>‘ sign symbolizes ‘greater than’). On the other hand, a T-independent extrafollicular response is not reliant on LDHA-mediated glycolysis.

Supplementary Material

Refer to Web version on PubMed Central for supplementary material.

Acknowledgements

R.S. was supported by the National Cancer Institute (U54CA137788); J.C. was supported by grants from the National Institutes of Health (R01AI072194 and R01AI124186) and from the National Cancer Institute (U54CA137788 and P30CA008748), the Starr Cancer Research Foundation, the Ludwig Center for Cancer Immunotherapy, MSKCC Functional Genomics and the Geoffrey Beene Cancer Center. M.O.L. was supported by a grant from the National Institutes of Health R01 (AI 102888). This work was supported in part by a grant from the Tri-Institutional Metabolomics Training Program (R25 AI140472) to J.R.C. J.R.C. is also supported by the Donald B. and Catherine C. Marron Cancer Metabolism Center. We thank A. Bravo for help with maintenance of the mouse colony. We thank all members of the laboratory of J.C. for helpful discussions and feedback. We acknowledge the use of the MSKCC Single-cell Analysis Innovation Lab for the generation of the scRNA-seq dataset and the Integrated Genomic Operation Core and the Molecular Cytology Core Facility at MSKCC supported by a Core Grant (P30CA008748).

Data availability

All sequencing data generated in this study are deposited at the Gene Expression Omnibus under the accession code GSE232660. All custom pipelines developed for analysis of scRNA-seq data and *Jh4* mutation data are available at https://github.com/ryashka/LDHA. Source data are provided with this paper.

References

1. Elsner RA & Shlomchik MJ Germinal center and extrafollicular B cell responses in vaccination, immunity, and autoimmunity. Immunity 53, 1136–1150 (2020). [PubMed: 33326765]
2. Mesin L, Ersching J & Victora GD Germinal center B cell dynamics. Immunity 45, 471–482 (2016). [PubMed: 27653600]
3. Roco JA et al. Class-switch recombination occurs infrequently in germinal centers. Immunity 51, 337–350 (2019). [PubMed: 31375460]
4. Chang CH et al. Posttranscriptional control of T cell effector function by aerobic glycolysis. Cell 153, 1239–1251 (2013). [PubMed: 23746840]
5. Lunt SY & Vander Heiden MG Aerobic glycolysis: meeting the metabolic requirements of cell proliferation. Annu. Rev. Cell Dev. Biol. 27, 441–464 (2011). [PubMed: 21985671]
6. O’Neill LA, Kishton RJ & Rathmell J A guide to immunometabolism for immunologists. Nat. Rev. Immunol. 16, 553–565 (2016). [PubMed: 27396447]
7. Warburg O, Gawehn K & Geissler AW Metabolism of leukocytes. Z. Naturforsch. B 13B, 515–516 (1958). [PubMed: 13593654]
8. Peng M et al. Aerobic glycolysis promotes T helper 1 cell differentiation through an epigenetic mechanism. Science 354, 481–484 (2016). [PubMed: 27708054]
9. Vander Heiden MG, Cantley LC & Thompson CB Understanding the Warburg effect: the metabolic requirements of cell proliferation. Science 324, 1029–1033 (2009). [PubMed: 19460998]
10. Xu K et al. Glycolysis fuels phosphoinositide 3-kinase signaling to bolster T cell immunity. Science 371, 405–410 (2021). [PubMed: 33479154]
11. Wu L et al. Niche-selective inhibition of pathogenic Th17 cells by targeting metabolic redundancy. Cell 182, 641–654 (2020). [PubMed: 32615085]

12. Xu K et al. Glycolytic ATP fuels phosphoinositide 3-kinase signaling to support effector T helper 17 cell responses. Immunity 54, 976–987 (2021). [PubMed: 33979589]
13. Crotty S T follicular helper cell differentiation, function, and roles in disease. Immunity 41, 529–542 (2014). [PubMed: 25367570]
14. Akkaya M & Pierce SK From zero to sixty and back to zero again: the metabolic life of B cells. Curr. Opin. Immunol. 57, 1–7 (2019). [PubMed: 30312894]
15. Caro-Maldonado A et al. Metabolic reprogramming is required for antibody production that is suppressed in anergic but exaggerated in chronically BAFF-exposed B cells. J. Immunol. 192, 3626–3636 (2014). [PubMed: 24616478]
16. Doughty CA et al. Antigen receptor-mediated changes in glucose metabolism in B lymphocytes: role of phosphatidylinositol 3-kinase signaling in the glycolytic control of growth. Blood 107, 4458–4465 (2006). [PubMed: 16449529]
17. Woodland RT et al. Multiple signaling pathways promote B lymphocyte stimulator dependent B cell growth and survival. Blood 111, 750–760 (2008). [PubMed: 17942753]
18. Jellusova J et al. Gsk3 is a metabolic checkpoint regulator in B cells. Nat. Immun. 18, 303–312 (2017).
19. Cho SH et al. Germinal centre hypoxia and regulation of antibody qualities by a hypoxia response system. Nature 537, 234–238 (2016). [PubMed: 27501247]
20. Weisel FJ et al. Germinal center B cells selectively oxidize fatty acids for energy while conducting minimal glycolysis. Nat. Immunol. 21, 331–342 (2020). [PubMed: 32066950]
21. Haniuda K, Fukao S & Kitamura D Metabolic reprogramming induces germinal center B cell differentiation through Bcl6 locus remodeling. Cell Rep. 33, 108333 (2020). [PubMed: 33147467]
22. Chen D et al. Coupled analysis of transcriptome and BCR mutations reveals role of OXPHOS in affinity maturation. Nat. Immunol. 22, 904–913 (2021). [PubMed: 34031613]
23. Waters LR, Ahsan FM, Wolf DM, Shirihai O & Teitell MA Initial B cell activation induces metabolic reprogramming and mitochondrial remodeling. iScience 5, 99–109 (2018). [PubMed: 30240649]
24. Price MJ, Patterson DG, Scharer CD & Boss JM Progressive upregulation of oxidative metabolism facilitates plasmablast differentiation to a T-independent antigen. Cell Rep. 23, 3152–3159 (2018). [PubMed: 29898388]
25. Hosios AM & Vander Heiden MG The redox requirements of proliferating mammalian cells. J. Biol. Chem. 293, 7490–7498 (2018). [PubMed: 29339555]
26. Kwon K et al. Instructive role of the transcription factor E2A in early B lymphopoiesis and germinal center B cell development. Immunity 28, 751–762 (2008). [PubMed: 18538592]
27. Chaudhuri J & Alt FW Class-switch recombination: interplay of transcription, DNA deamination and DNA repair. Nat. Rev. Immunol. 4, 541–552 (2004). [PubMed: 15229473]
28. Zdralevic M et al. Double genetic disruption of lactate dehydrogenases A and B is required to ablate the ‘Warburg effect’ restricting tumor growth to oxidative metabolism. J. Biol. Chem. 293, 15947–15961 (2018). [PubMed: 30158244]
29. Allman D et al. Resolution of three nonproliferative immature splenic B cell subsets reveals multiple selection points during peripheral B cell maturation. J. Immunol. 167, 6834–6840 (2001). [PubMed: 11739500]
30. Peng SL Signaling in B cells via Toll-like receptors. Curr. Opin. Immunol. 17, 230–236 (2005). [PubMed: 15886111]
31. Barwick BG, Scharer CD, Bally APR & Boss JM Plasma cell differentiation is coupled to division-dependent DNA hypomethylation and gene regulation. Nat. Immunol. 17, 1216–1225 (2016). [PubMed: 27500631]
32. Tangye SG, Bryant VL, Cuss AK & Good KL BAFF, APRIL and human B cell disorders. Semin. Immunol. 18, 305–317 (2006). [PubMed: 16916610]
33. Boothby M & Rickert RC Metabolic regulation of the immune humoral response. Immunity 46, 743–755 (2017). [PubMed: 28514675]
34. Reboldi A & Cyster JG Peyer’s patches: organizing B-cell responses at the intestinal frontier. Immunol. Rev. 271, 230–245 (2016). [PubMed: 27088918]

35. Jacob J, Kelsoe G, Rajewsky K & Weiss U Intraclonal generation of antibody mutants in germinal centres. Nature 354, 389–392 (1991). [PubMed: 1956400]
36. Reimer D et al. Early CCR6 expression on B cells modulates germinal centre kinetics and efficient antibody responses. Immunol. Cell Biol. 95, 33–41 (2017). [PubMed: 27465674]
37. Schwickert TA et al. A dynamic T cell-limited checkpoint regulates affinity-dependent B cell entry into the germinal center. J. Exp. Med. 208, 1243–1252 (2011). [PubMed: 21576382]
38. Jacobsen JT et al. Expression of Foxp3 by T follicular helper cells in end-stage germinal centers. Science 373, eabe5146 (2021).
39. Ganeshan K & Chawla A Metabolic regulation of immune responses. Annu. Rev. Immunol. 32, 609–634 (2014). [PubMed: 24655299]
40. Robbiani DF et al. AID is required for the chromosomal breaks in c-myc that lead to c-myc/IgH translocations. Cell 135, 1028–1038 (2008). [PubMed: 19070574]
41. Jolly CJ, Klix N & Neuberger MS Rapid methods for the analysis of immunoglobulin gene hypermutation: application to transgenic and gene targeted mice. Nucleic Acids Res. 25, 1913–1919 (1997). [PubMed: 9115357]
42. Sheppard S et al. Lactate dehydrogenase A-dependent aerobic glycolysis promotes natural killer cell anti-viral and anti-tumor function. Cell Rep. 35, 109210 (2021). [PubMed: 34077737]
43. DeFranco AL, Raveche ES & Paul WE Separate control of B lymphocyte early activation and proliferation in response to anti-IgM antibodies. J. Immunol. 135, 87–94 (1985). [PubMed: 3873499]
44. Dominguez-Sola D et al. The proto-oncogene MYC is required for selection in the germinal center and cyclic reentry. Nat. Immunol. 13, 1083–1091 (2012). [PubMed: 23001145]
45. Schuhmacher M et al. Control of cell growth by c-Myc in the absence of cell division. Curr. Biol. 9, 1255–1258 (1999). [PubMed: 10556095]
46. Kwak K, Akkaya M & Pierce SK B cell signaling in context. Nat. Immunol. 20, 963–969 (2019). [PubMed: 31285625]
47. Zhang D et al. Metabolic regulation of gene expression by histone lactylation. Nature 574, 575–580 (2019). [PubMed: 31645732]
48. Fagone P et al. Phospholipid biosynthesis program underlying membrane expansion during B-lymphocyte differentiation. J. Biol. Chem. 282, 7591–7605 (2007). [PubMed: 17213195]
49. Goldfinger M et al. De novo ceramide synthesis is required for N-linked glycosylation in plasma cells. J. Immunol. 182, 7038–7047 (2009). [PubMed: 19454701]
50. Kirk SJ, Cliff JM, Thomas JA & Ward TH Biogenesis of secretory organelles during B cell differentiation. J. Leukoc. Biol. 87, 245–255 (2010). [PubMed: 19889725]
51. Wiest DL et al. Membrane biogenesis during B cell differentiation: most endoplasmic reticulum proteins are expressed coordinately. J. Cell Biol. 110, 1501–1511 (1990). [PubMed: 2335560]
52. Dufort FJ et al. Glucose-dependent de Novo Lipogenesis in B Lymphocytes. J. Bio. Chem. 289, 7011–7024 (2014). [PubMed: 24469453]
53. Lam WY et al. Mitochondrial pyruvate import promotes long-term survival of antibody-secreting plasma cells. Immunity 45, 60–73 (2016). [PubMed: 27396958]
54. Muschen M Metabolic gatekeepers to safeguard against autoimmunity and oncogenic B cell transformation. Nat. Rev. Immunol. 19, 337–348 (2019). [PubMed: 30890785]
55. Lee PP et al. A critical role for Dnmt1 and DNA methylation in T cell development, function, and survival. Immunity 15, 763–774 (2001). [PubMed: 11728338]
56. Sage PT & Sharpe AH In vitro assay to sensitively measure T_{FR} suppressive capacity and T_{FH} stimulation of B cell responses. Methods Mol. Biol. 1291, 151–160 (2015). [PubMed: 25836309]
57. Yewdell WT et al. A Hyper-IgM syndrome mutation in activation-induced cytidine deaminase disrupts G-Quadruplex binding and genome-wide chromatin localization. Immunity 53, 952–970 (2020). [PubMed: 33098766]
58. Yewdell WT et al. Temporal dynamics of persistent germinal centers and memory B cell differentiation following respiratory virus infection. Cell Rep. 37, 109961 (2021). [PubMed: 34758310]

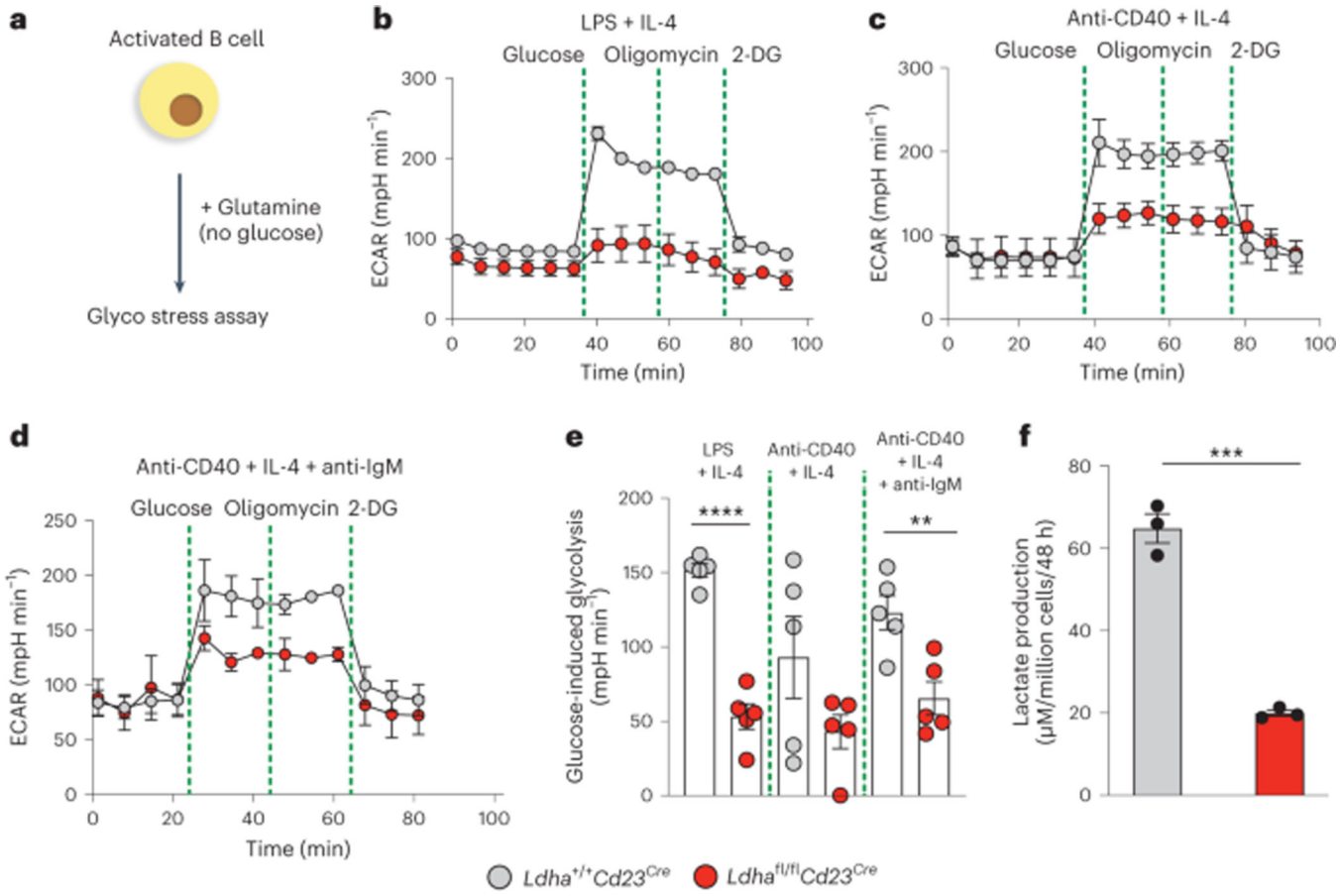

Fig. 1 |. LDHA governs aerobic glycolysis in B cells.

a, Schematic representation of a glycolysis stress assay performed in a Seahorse analyzer. During this assay, ECAR is first measured when cells are grown in media without glucose, and then measured after the sequential addition of glucose (which is converted into lactate leading to acidification of the media), oligomycin (which inhibits mitochondrial respiration) and 2-deoxyglucose (2-DG; a glucose analog that inhibits glycolysis). **b**–**d**, Representative graphs showing ECAR of naïve B cells activated with LPS + IL-4 (b), anti-CD40 + IL-4 (c) or anti-CD40 + IL-4 + anti-IgM (d) for 48 h. Cells were cultured in glucose-deprived Seahorse minimal media for 30–40 min before glycolytic flux analysis. The time point at which glucose, oligomycin and 2-DG are added to the cells is indicated by the dashed green line. **e**, Quantification of glucose-induced glycolysis in B cells activated ex vivo as indicated. Glycolysis was measured as the difference of maximum ECAR after glucose injection and minimum ECAR after 2-DG treatment. **f**, Lactate produced by B cells after 48 h of culture with LPS + IL-4. $n = 5$ for each genotype except for **f** wherein n = 3 for each group; data were pooled from three independent experiments. Bars represent the mean ± s.e.m.; $^{**}P \leq 0.01$, $^{***}P \leq 0.001$, $^{****}P \leq 0.0001$ by unpaired, two-tailed *t*-test.

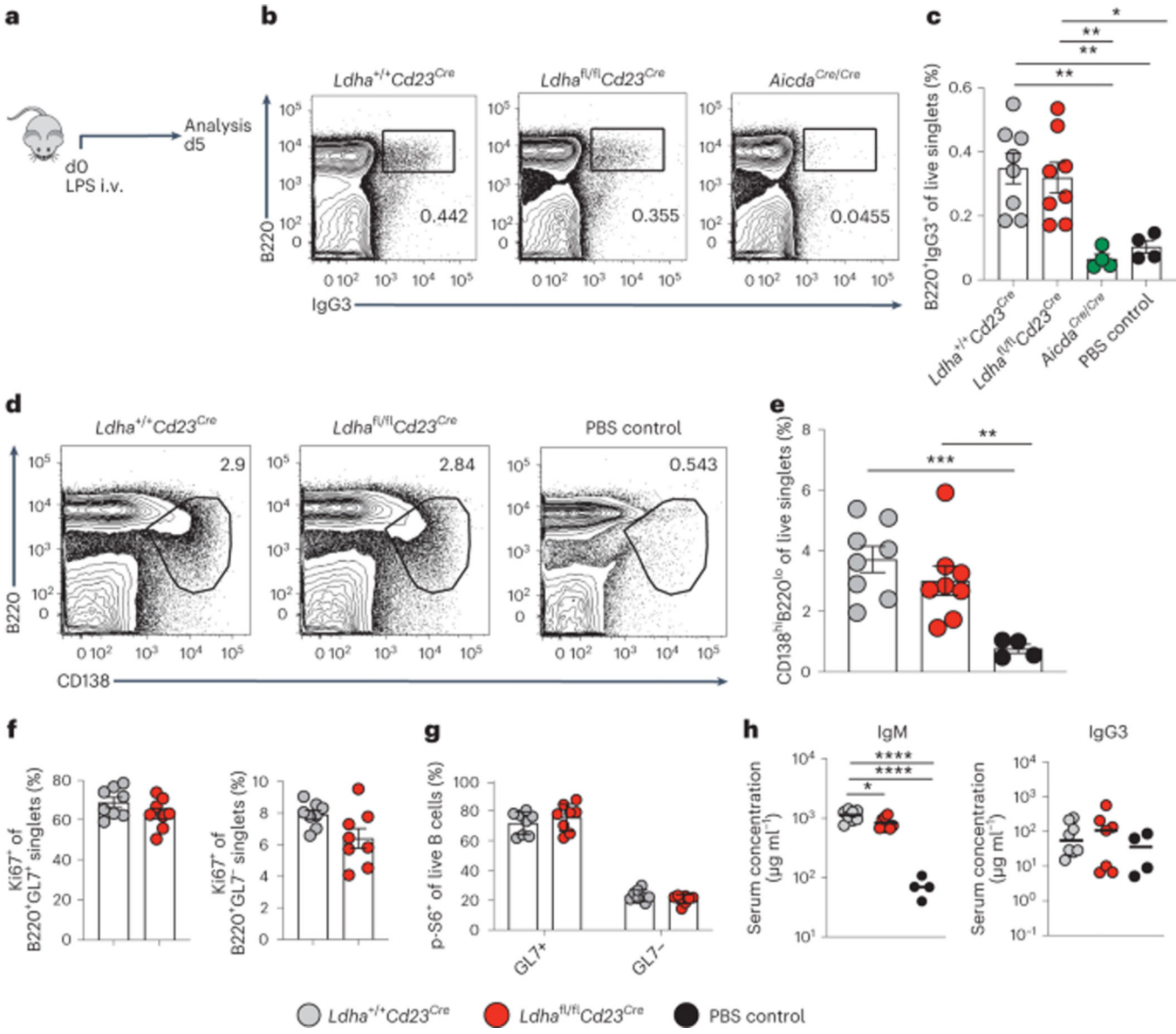

Fig. 2 |. LDHA is dispensable for lipopolysaccharide-dependent extrafollicular responses.

a, Schematic of experimental strategy. Mice intravenously (i.v.) injected with LPS or PBS were analyzed at d5. **b**,**c**, Representative flow cytometry plots (**b**) and quantification (**c**) of class-switched IgG3^{+} B cells gated among live singlets in the spleen of LPS-injected *Ldha*$^{+/+}$*Cd23*^{Cre} (control, $n = 8$), *Ldha*$^{fl/fl}$ *Cd23*^{Cre} ($n = 8$), *Aicda*$^{Cre/Cre}$ (used as an AID knockout control, $n = 4$) and PBS-injected ($n = 4$) mice. Data are representative of three independent experiments. **d**,**e**, Representative flow cytometry plots (**d**) and quantification (**e**) of plasmablasts (B220^{lo}CD138^{hi}) among live singlets in *Ldha*$^{+/+}$*Cd23*^{Cre} ($n = 8$), *Ldha*$^{fl/fl}$ *Cd23*^{Cre} ($n = 8$) and PBS-injected ($n = 4$) mice. Data are representative of three independent experiments. **f**, Quantification of cell proliferation in activated (GL7^{+}) and unactivated (GL7^{-}) B cells as assessed by Ki67 staining ($n = 8$ for each group). **g**, mTORC1 activity quantified as the frequency of phosphorylated S6 (p-S6) in activated (GL7^{+}) and unactivated (GL7^{-}) B cells. Data are representative of three independent experiments, with $n = 8$ for

each group. **h**, Concentrations of IgM and IgG3 antibodies at d5 after LPS administration. For LPS-injected animals, $n = 8$ for each group, except for $Ldha^{fl/fl}Cd23^{Cre}$ mice that were examined for IgG3 antibodies, $n = 7$; PBS-injected mice, $n = 4$. Bars represent the mean in **h** and the mean ± s.e.m. for all other graphs. $*P \leq 0.05$, $**P \leq 0.01$, $***P \leq 0.001$, $****P \leq 0.0001$ by unpaired, two-tailed *t*-test.

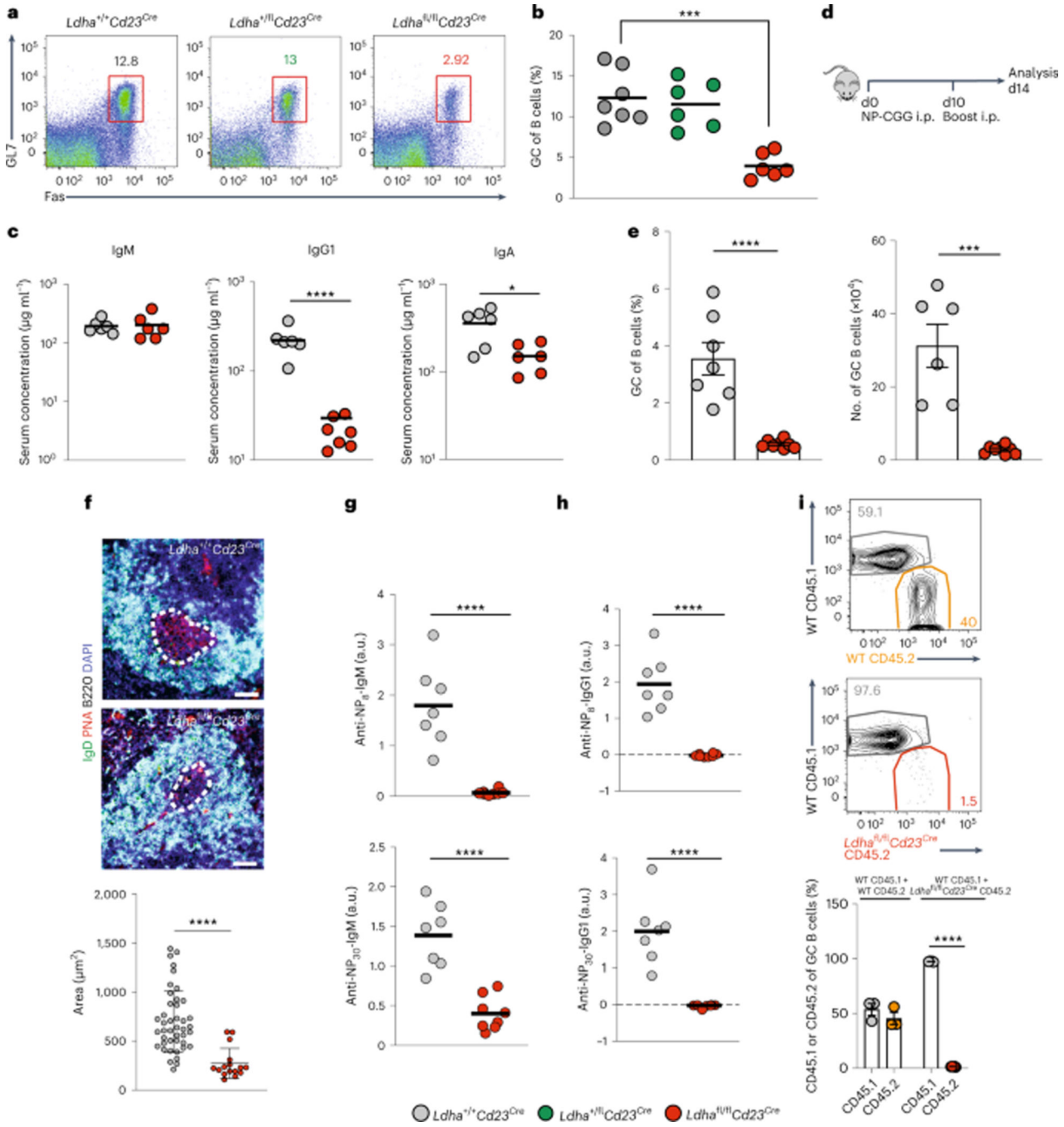

Fig. 3 |. Loss of LDHA in naïve B cells impairs germinal center responses.

a–**c**, GC response at homeostasis. **a**, Representative flow plots (**a**) and quantification (**b**) of GC B cell frequencies in the PPs of *Ldha*$^{+/+}$*Cd23*^{Cre} (*n* = 7), *Ldha*$^{+/fl}$*Cd23*^{Cre} (*n* = 6) and *Ldha*$^{fl/fl}$*Cd23*^{Cre} (*n* = 6) mice. **c**, Serum antibody titers of IgM, IgG1 and IgA isotypes in *Ldha*$^{+/+}$*Cd23*^{Cre} (*n* = 6) and *Ldha*$^{fl/fl}$*Cd23*^{Cre} (*n* = 6, except for serum IgG1 measurement in which *n* = 7) mice at homeostasis. **d**,**e**, GC response following NP-CGG immunization. **d**, Schematic of NP-CGG immunization. Mice were immunized intraperitoneally (i.p.) with NP-CGG, boosted at d10 and analyzed at d14. **e**, The frequency (*n* = 7 for *Ldha*$^{+/+}$*Cd23*^{Cre}

and $n = 8$ for $Ldha^{fl/fl}Cd23^{Cre}$) and absolute number ($n = 6$ for $Ldha^{+/+}Cd23^{Cre}$ and $n = 8$ for $Ldha^{fl/fl}Cd23^{Cre}$) of GC B cells were quantified in the spleens of immunized mice of the indicated genotypes at d14. **f**, Representative immunofluorescence staining and quantification of GC area in spleen sections from mice of the indicated genotypes at d14 after immunization. Data are representative of three mice of each genotype. Scale bar, 50 μm. **g**, Relative titers of high-affinity (NP_8) and all-affinity (NP_{30}) anti-NP IgM antibodies at d14 after immunization ($n = 7$ for $Ldha^{+/+}Cd23^{Cre}$ and $n = 8$ for $Ldha^{fl/fl}Cd23^{Cre}$ mice). **h**, Relative titers of high-affinity (anti-NP_8) and all-affinity (anti-NP_{30}) anti-NP IgG1 antibodies at d14 after immunization ($n = 8$ for mice of each genotype). **i**, Bone marrow from wild-type (WT; CD45.1) or $Ldha^{fl/fl}Cd23^{Cre}$ mice (CD45.2) were mixed at a 1:1 ratio, transplanted into γ-irradiated RAG2-deficient recipient mice. Following 8 weeks of reconstitution, mice were immunized with NP-CGG as described above and analyzed. Reconstitution experiments with CD45.1 and CD45.2 wild-type bone marrow cells mixed at a 1:1 ratio served as controls. Representative flow plots and quantification of congenically marked GC B cells ($GL7^+Fas^+$ of live $B220^+$ B cells) in the spleens of immunized mice are shown. $n = 3$ for CD45.1 and $n = 5$ for CD45.2 mice. Bars represent the mean ± s.e.m. for all the graphs except in **c**, **g** and **h** where bars indicate the mean; $^{**}P \leq 0.01$, $^{***}P \leq 0.001$, $^{****}P \leq 0.0001$ by unpaired, two-tailed *t*-test and by two-way analysis of variance (ANOVA) for **i**. a.u., arbitrary units.

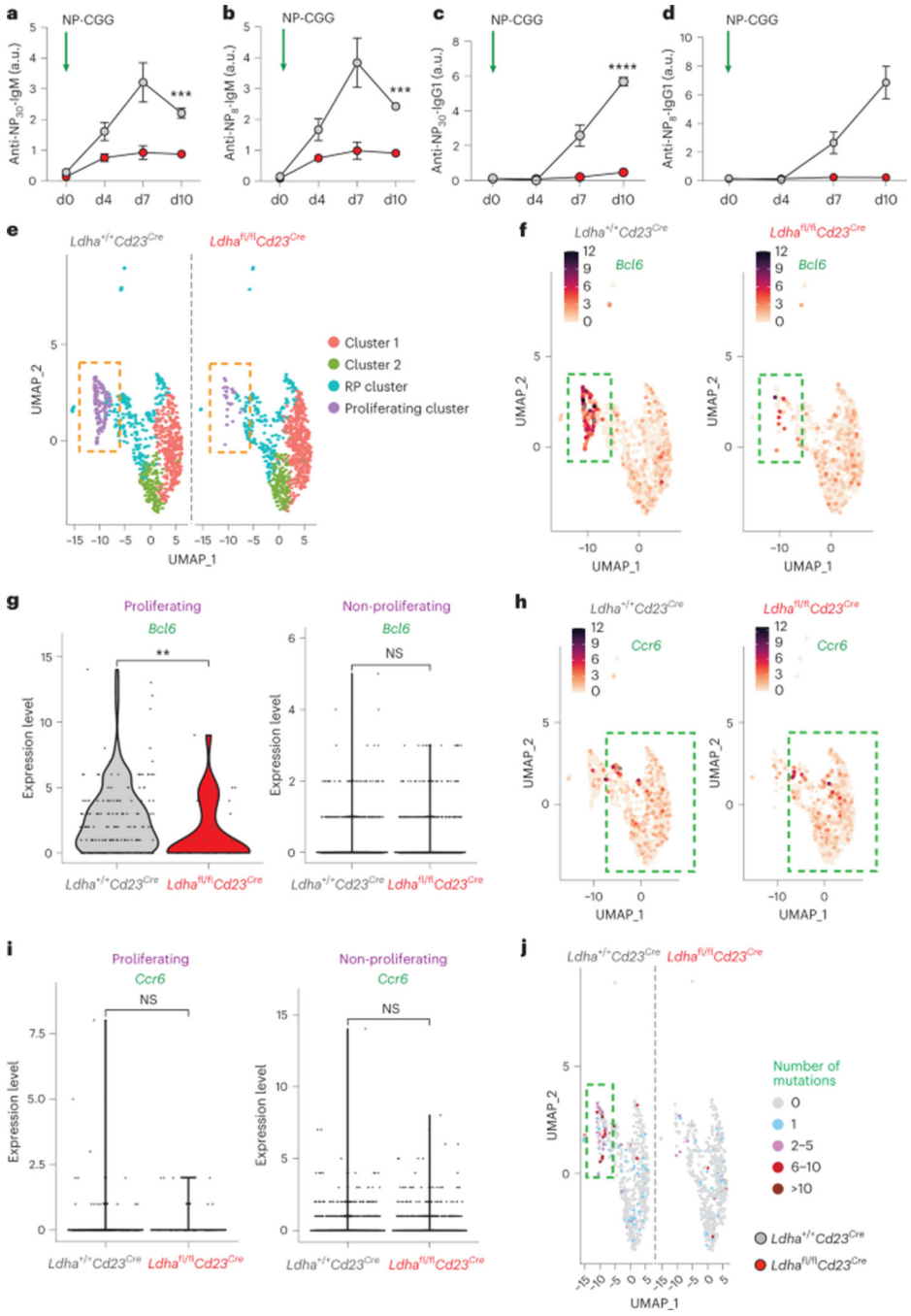

Fig. 4 |. LDHA is required for pre-germinal center B cell proliferation.

a–**d**, Analysis of pre-GC B cells antibody responses by single-dose immunization of NP-CGG measuring serum titers at d0 (pre-immunization), d4, d7 and d10. The green arrow indicates the time point for immunization. $n = 4$ animals for each indicated genotype.

e–**j**, Single-cell transcriptome and BCR mutation analysis of pre-GC B cells. Mice (*Ldha*$^{+/+}$*Cd23*^{Cre} or *Ldha*$^{fl/fl}$*Cd23*^{Cre}) were immunized with NP-CGG and at d4 after immunization. GL7^{+} (activated) and GL^{-} (naïve) B cells from the spleen of indicated genotypes were enriched, mixed at a 3:1 ratio and subjected to single-cell BCR and transcriptome analysis.

e, Uniform manifold approximation and projection (UMAP) of B cells from mice of the indicated genotypes. Of the four clusters, only the proliferating cluster, defined by the expression of *Mki67* and *Top2a*, was markedly reduced in *Ldha*$^{fl/fl}$*Cd23*^{Cre} mice. RP, ribosomal protein. **f**,**g**, UMAP analysis of *Bcl6* expression in pre-GC B cells of *Ldha*$^{fl/fl}$*Cd23*^{Cre} and control mice. **g**, Violin plots for *Bcl6* expression in proliferating and non-proliferating pre-GC B cells. **h**,**i**, UMAP analysis of *Ccr6* expression in pre-GC B cells of *Ldha*$^{fl/fl}$*Cd23*^{Cre} and control mice. **i**, Violin plots for *Ccr6* expression in proliferating and non-proliferating pre-GC B cells. **j**, Total number of mutations in the immunoglobulin heavy chain (*IgH*) of pre-GC B cells. For **a**–**d**, data points represent the mean ± s.d. $^{**}P \leq 0.01$, $^{***}P \leq 0.001$, by two-way ANOVA. NS, not significant.

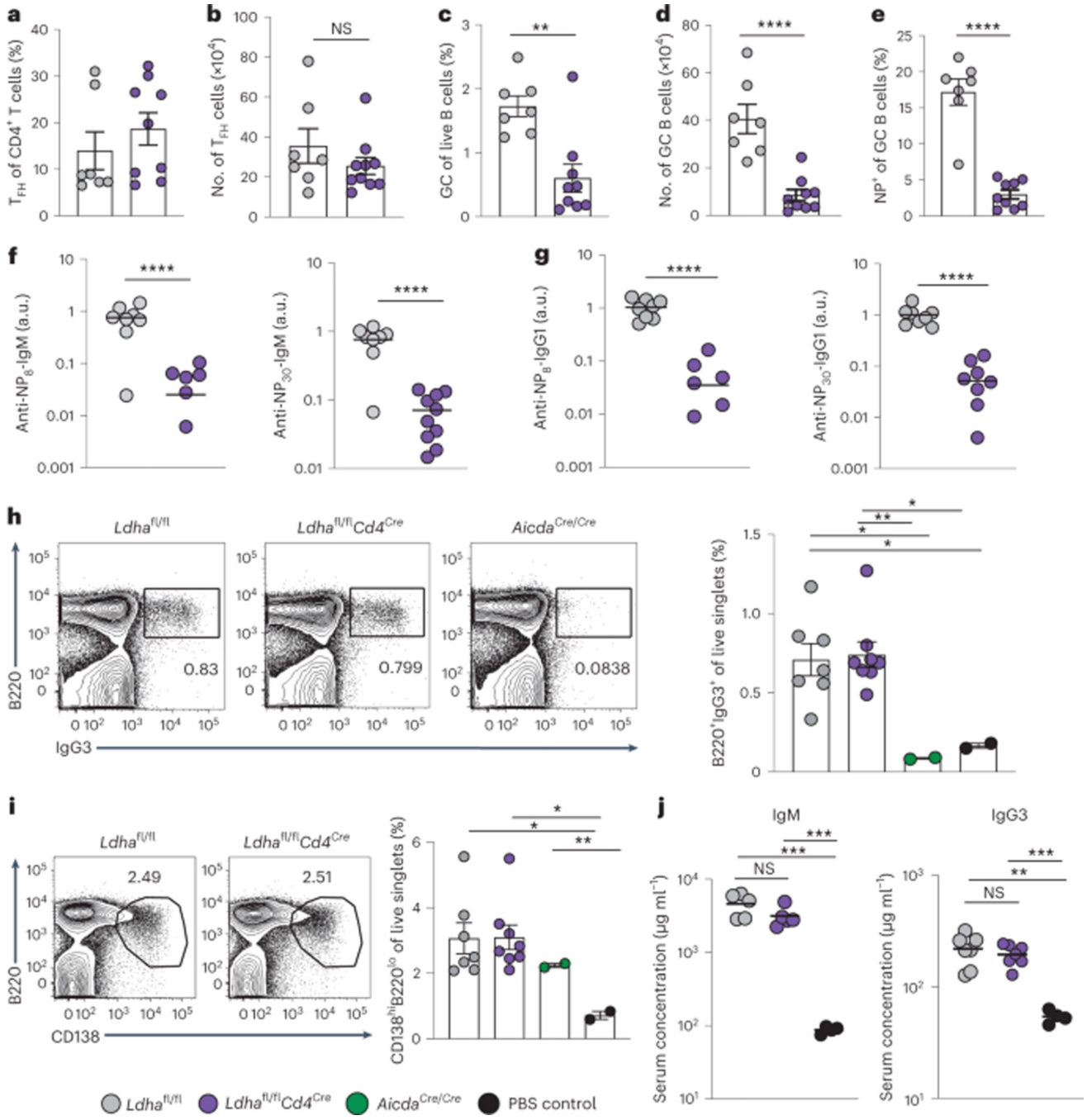

Fig. 5 |. LDHA in T cells regulates germinal B cell responses.

a–**g**, *Ldha*$^{fl/fl}$ and *Ldha*$^{fl/fl}$*Cd4*^{Cre} mice were immunized intraperitoneally with NP-CGG, boosted at d10, and analyzed at d14. **a**,**b**, Frequency (**a**) and absolute number (**b**) of T_{FH} cells ($PD1^+CXCR5^+$ gated among live singlet $B220^-CD3^+CD4^+CD44^+$ cells) in the spleens of immunized mice. **c**,**d**, Frequency (**c**) and absolute number (**d**) of GC B cells in the spleens of immunized mice. **e**, Frequency of NP^+ B cells within the GC population. **f**, Relative titers of high-affinity (NP_8) and all-affinity (NP_{30}) anti-NP IgM antibodies at d14 after immunization. **g**, Relative titers of high-affinity (anti-NP_8) and all-affinity (anti-NP_{30})

anti-NP IgG1 antibodies at d14 after immunization. **h**–**j**, *Ldha*$^{fl/fl}$, *Ldha*$^{fl/fl}$*Cd4*^{Cre} and *Aicda*$^{Cre/Cre}$ (AID knockout) mice were intravenously injected with LPS or PBS (control) and analyzed at d5. **h**, Representative flow plots and quantification showing IgG3^{+} B cells. **i**, Representative flow plots and quantification of plasmablasts (B220^{lo}CD138^{hi}) in the spleens of LPS-challenged mice. **j**, Absolute serum titers of IgM and IgG3 at d5 after LPS administration. Bars represent the mean for **f**, **g** and **j** and the mean ± s.e.m. for all other graphs. *$P \leq 0.05$, **$P \leq 0.01$, ***$P \leq 0.001$, ****$P \leq 0.0001$ by unpaired, two-tailed *t*-test. In **a**–**e**, $n = 7$ for *Ldha*$^{fl/fl}$ and $n = 9$ for *Ldha*$^{fl/fl}$*Cd4*^{Cre} mice; in **f** and **g**, $n = 8$ for *Ldha*$^{fl/fl}$ and $n = 10$ for *Ldha*$^{fl/fl}$*Cd4*^{Cre} mice, although some of these datapoints fell below the detection limit of the assay and thus were not plotted (4 for anti-NP_8 IgM and IgG1 titer measurements, and 2 for anti-NP_{30} IgG1 titer measurement); in **h** and **i**, $n = 7$ *Ldha*$^{fl/fl}$ and $n = 8$ for *Ldha*$^{fl/fl}$*Cd4*^{Cre} mice; in **j**, n = 5 for each group (IgM antibody titer) and $n = 7$ for each group (IgG3 antibody titer). All data are representative of three independent experiments.

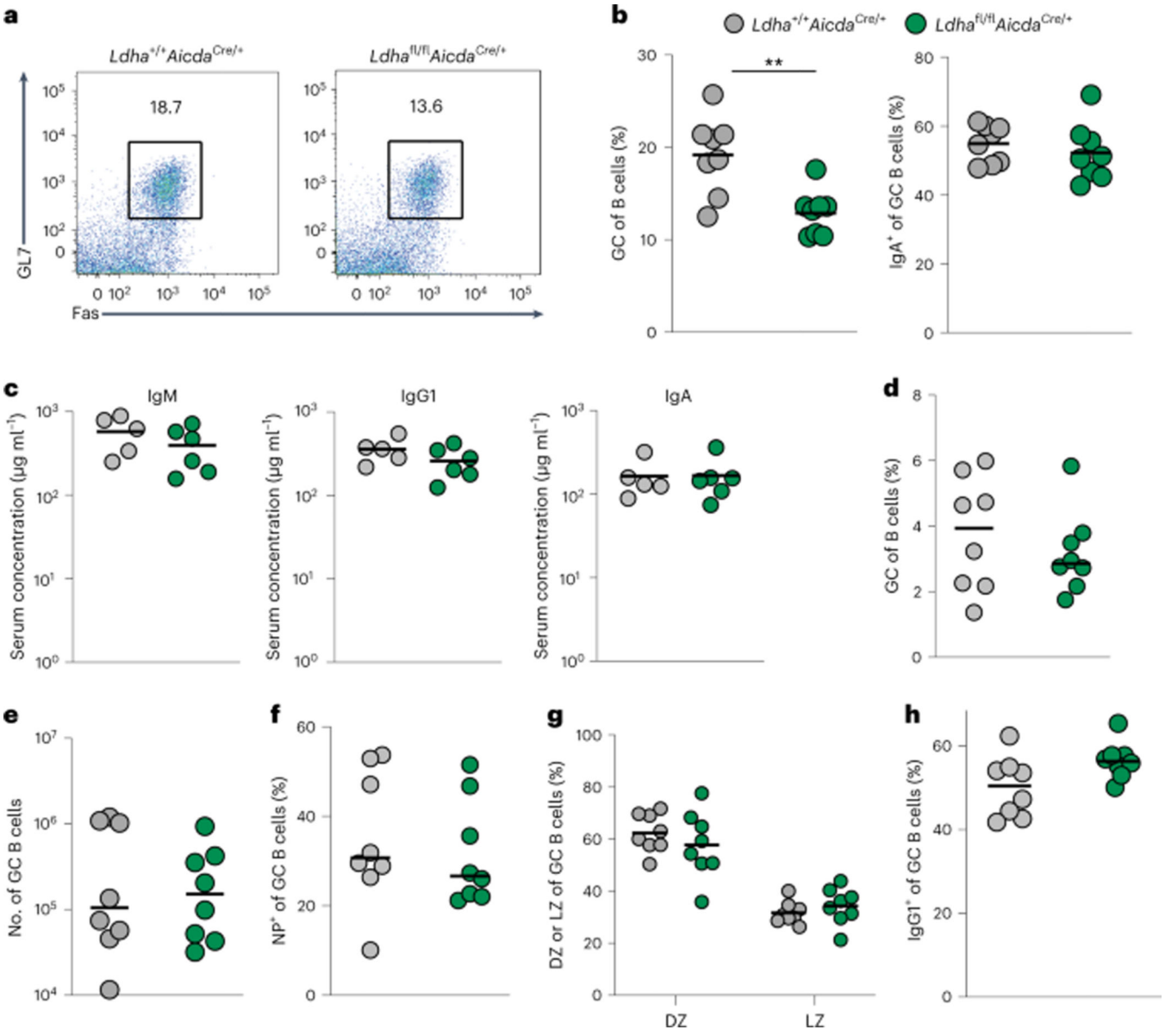

Fig. 6 |. LDHA is largely dispensable for germinal center responses after B cell activation.

a,**b**, PPs of *Ldha*$^{+/+}$*Aicda*$^{Cre/+}$ and *Ldha*$^{fl/fl}$*Aicda*$^{Cre/+}$ mice. **a**, Representative flow plots of GC B cells (GL7^{+}Fas^{+} of live B220^{+} B cells). **b**, Frequency of GC B cells and frequency of IgA^{+} B cells within the GC population (n = 8 for each group). Data are representative of two independent experiments. **c**, Concentration of IgM, IgG1 and IgA antibodies in the sera of *Ldha*$^{+/+}$*Aicda*$^{Cre/+}$ (n = 5) and *Ldha*$^{fl/fl}$*Aicda*$^{Cre/+}$ (n = 6) mice at homeostasis. **d**–**h**, Mice of the indicated genotypes (n = 8 animals per group) were immunized with NP-CGG, boosted at d10 and analyzed at d14. **d**,**e**, Frequency (**d**) and absolute number (**e**) of GC B cells in the spleens of immunized mice. **f**, Frequency of NP^{+} B cells among the GC B cell population in the spleens of immunized mice. **g**, Frequencies of DZ (CXCR4^{hi} CD86^{lo} of GC B cells) and LZ (CXCR4^{lo} CD86^{hi} of GC B cells) GC B cells. **h**, Frequency of IgG1^{+} class-switched

B cells in the splenic GCs of immunized mice. Data are representative of two independent experiments.

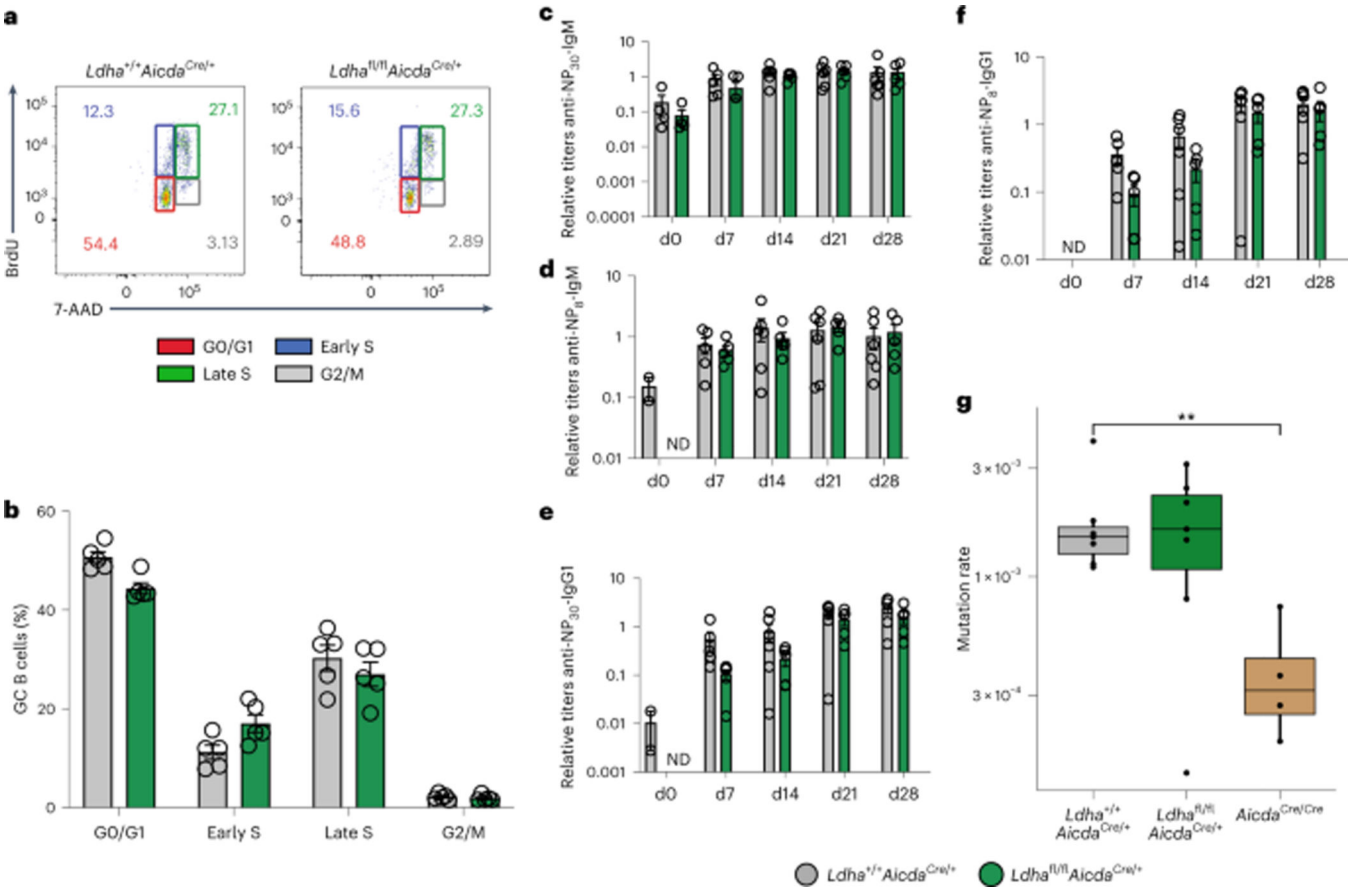

Fig. 7 |. Activated B cells do not rely on LDHA for affinity maturation.

Mice of the indicated phenotypes were immunized with NP-CGG, boosted at d10 and analyzed at d14. **a**,**b**, Cell-cycle analysis of GC B cells. **a**, Representative flow plots of BrdU incorporation versus total DNA stained with 7-AAD, gated on GC B cells. **b**, Quantification of the fractions of GC B cells at the different stages of the cell cycle ($n = 5$). Data are representative of two independent experiments. **c**,**d**, Measurement of all-affinity (anti-NP_{30}) (**c**) and high-affinity (anti-NP_8) (**d**) anti-NP IgM antibodies at indicated time points. **e**,**f**, Measurement of all-affinity (anti-NP_{30}) (**e**) and high-affinity (anti-NP_8) (**f**) anti-NP IgG1 antibodies at the indicated time points. Data for **c**–**f** are representative of two independent experiments ($n = 5$ for $Ldha^{+/+}Aicda^{Cre/+}$, $n = 6$ for $Ldha^{fl/fl}Aicda^{Cre/+}$ mice). **g**, Mutations detected by JH4 intron sequencing in GC B cells sorted from $Ldha^{fl/fl}$ $Aicda^{Cre/+}$ ($n = 6$) and $Ldha^{+/+}Aicda^{Cre/+}$ ($n = 5$) mice. Data are representative of two independent experiments. Bars represent the mean and mean ± s.e.m, wherever applicable. $^{**}P \leq 0.01$, by unpaired, two-tailed *t*-test. ND, not detectable. In the box plot (**g**), the top and bottom edges of the box correspond to the first and third quartiles, the middle line denotes the median and the whiskers represent the largest and smallest values no greater than 1.5 times the interquartile range. Outliers are plotted as individual points outside the boundary of the whiskers.